MSDE IChemE ADVANCING CHEMICAL ENGINEERING WORLDWIDE

Electrochemically mediated deionization: a review

Journal:	*Molecular Systems Design & Engineering*
Manuscript ID	ME-REV-07-2020-000090.R1
Article Type:	Review Article
Date Submitted by the Author:	21-Oct-2020
Complete List of Authors:	Suresh, Adarsh; University of Chicago Hill, Grant; University of Chicago Hoenig, Eli; University of Chicago Liu, Chong; University of Chicago, Pritzker School of Molecular Engineering

SCHOLARONE™
Manuscripts

Electrochemically mediated deionization: a review

Adarsh Suresh[1*], Grant Hill[1*], Eli Hoenig[1*], Chong Liu[1†]

[1]Pritzker School of Molecular Engineering, University of Chicago, 5640 S Ellis Ave, Chicago, IL 60637
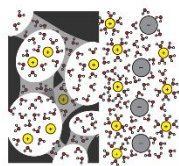
[†]Correspondence should be addressed to C.L. (chongliu@uchicago.edu)

[*]These authors contributed equally. The sequence appears as a result of flip coins outcomes.

Design, System, Application Statement

Global water shortages and strategic resource scarcities have spurred efforts to efficiently purify water and extract valuable elements from aqueous solutions. The growing market penetration of renewably generated electricity provides new opportunities to develop electrochemical methods for both applications. Here, we review the science and engineering principles of electrochemically mediated water desalination and selective ion extraction. We divide our review into four areas: Capacitive Deionization, Faradaic Desalination, Depletion Zone Desalination, and Selective Electrosorption. In each area, we detail electrode materials and device designs of novel and/or high-performing methods. Fundamental charge transfer mechanisms and ion interactions at the solid-water interface are also discussed in order to provide insights for further technology development.
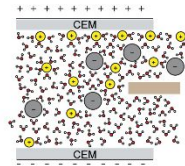
A review detailing existing electrode materials, cell architectures, and charge transfer mechanisms related to electrochemically driven desalination and selective element extraction in aqueous environments.
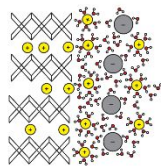
CDI/Selective CDI   Faradaic Insertion   Depletion Zone Desalination

Electrochemically mediated deionization: a review

Adarsh Suresh[1*], Grant T. Hill[1*], Eli Hoenig[1*], Chong Liu[1†]

[1]Pritzker School of Molecular Engineering, University of Chicago, 5640 S Ellis Ave, Chicago, IL 60637

[†]Correspondence should be addressed to C.L. (chongliu@uchicago.edu)

[*]These authors contributed equally. The sequence appears as a result of flip coins outcomes.

Abstract

Electrochemical deionization technologies allow generation of potable water from contaminated sources and extraction of valuable resources from seawater, brines and industrial wastewater—all in an environmentally friendly and energy efficient manner. In this review, we detail existing electrode materials, cell architectures, and charge transfer mechanisms related to electrochemically driven desalination and selective element extraction in aqueous environments. More specifically, we address capacitive and faradaic charge-transfer processes—ion electrosorption and ion intercalation, respectively. We also address selective electrosorption/electrodeposition at functionalized electrode surfaces. The selectivity is driven by ion specific interactions at the electrode, such as chelation and redox activity. Electrochemically mediated deionization strategies can help address the global need for potable water. Their widespread adoption hinges on a thorough understanding of the range of available deionization methods—which we attempt to provide in this review.

1. Introduction

As a result of rapid population growth and global development, the lack of clean and accessible water has become a critical international concern[1]. A small fraction of the earth's water is freshwater and much of this supply is inaccessible: <1% of all the water on the planet is readily available for human use[2]. Some arid, coastal and arctic regions are geographically limited in their access to freshwater, while other regions are plagued by environmental pollution from heavy metal contaminants such as lead, chromium, arsenic. With ongoing climate change, uncertainties concerning potable water access will only grow more severe.

Amid the limited supply of freshwater, the mounting pressures of a rising population, fast paced economic growth and technological development are resulting in heightening demand for crucial resources such as lithium (battery applications), uranium (nuclear energy production) and rare-earth elements (advanced consumer electronics and renewable energy technology). Extracting such sought after resources from seawater, brines and wastewater can mitigate the negative environmental impacts of traditional mining methods. Therefore, we are not only faced with the significant task of efficiently sourcing, treating and distributing water to high-stress regions of the world but also of securing strategic resources from dilute sources with minimal impact to environment.

All of the current desalination technologies are energy and capital intensive[3]: thermal distillation, one of the most common desalination methods, uses ~50 times more energy than the fundamental thermodynamic limit[4]. Non-thermal alternatives for desalination (e.g. reverse osmosis) are more efficient but remain costly to operate and maintain. While seawater reverse osmosis (SWRO) currently holds a majority share of the desalination market, likely a result of the >5 fold increase in energy efficiency since the 1970s[5], it still requires, on average, an order of magnitude more energy than freshwater treatment[6]. Environmentally, there are serious concerns surrounding the impacts of brine discharge on coastal ecosystems near SWRO plants, and the CO_2 emissions from SWRO plants are significant and unavoidable[7].

Electrochemical deionization processes that produce clean water from seawater, brackish water and brines have attracted a great deal of attention owing to their unique capabilities, environmental-friendliness and

3

cost-effectiveness: they can operate directly off renewably generated electricity and can operate efficiently at small scales[8]. At salt concentrations below ~10 g L^{-1}, the theoretical efficiency of electrochemically driven desalination surpasses that of reverse osmosis (RO)[9]. Moreover, certain applications such as toxic waste remediation and resource mining demand ion-selectivity. Ionic selectivity can be induced in electrochemical deionization processes with much higher capacity and kinetics relative to that of physicochemical adsorption, and with more flexibility than in pressure-driven separations due to the vast array of ion-selective electrodes and electrode coatings (described in Section 5 of this review).

In this review, the most prominent electrochemical deionization technologies are categorized into non-faradaic, faradaic, ion-depletion, and selective electrosorption/electrodeposition systems (Fig. 1). Capacitive deionization (CDI) and electrodialysis (ED) are among the earliest and most important examples of *non-faradaic* processes. In the most basic CDI process, ions and counterions are electrostatically attracted to their respective electrodes and adsorb on the surface to form regions of excess charge known as electrical double layers (EDL); this depletes the remaining solution of charged species and results in a deionized water stream (Fig. 1a). On the other hand, ED relies on the transport of ions through ion-exchange membranes (IEMs) that form deionized and brine streams partitioned by the membrane. In this review, we focus on CDI and refer the reader to several comprehensive reviews on the more mature ED systems[10–12].

All electrode materials have intrinsic physical properties that determine their performance in CDI applications: conductivity, surface area, pore-distribution and surface charge. Significant theoretical and experimental work has correlated microscopic physical properties to CDI performance, leading to great improvements in CDI technology[13–15]. Researchers have also altered and optimized CDI cell-architectures— such as flow through[8], flow-between[16–18] and flow electrode[19] type cells—each of which comes with their own tradeoffs, covered in detail in Section 2.3 of this review. The addition of ion-selective membranes to the CDI electrodes—the combination is called membrane CDI (MCDI)—has further driven the capacity and kinetics of CDI systems, as have direct chemical modifications of the electrode material[20,21]. While CDI is typically associated with desalination, selective CDI systems have also been

developed to separate monovalent and divalent ions based on principles of electrostatic interaction and size exclusion[22]. Modified CDI processes such as MCDI and hybrid CDI (HCDI, discussed below) have also been used for selective electrosorption of nitrates[23–26].
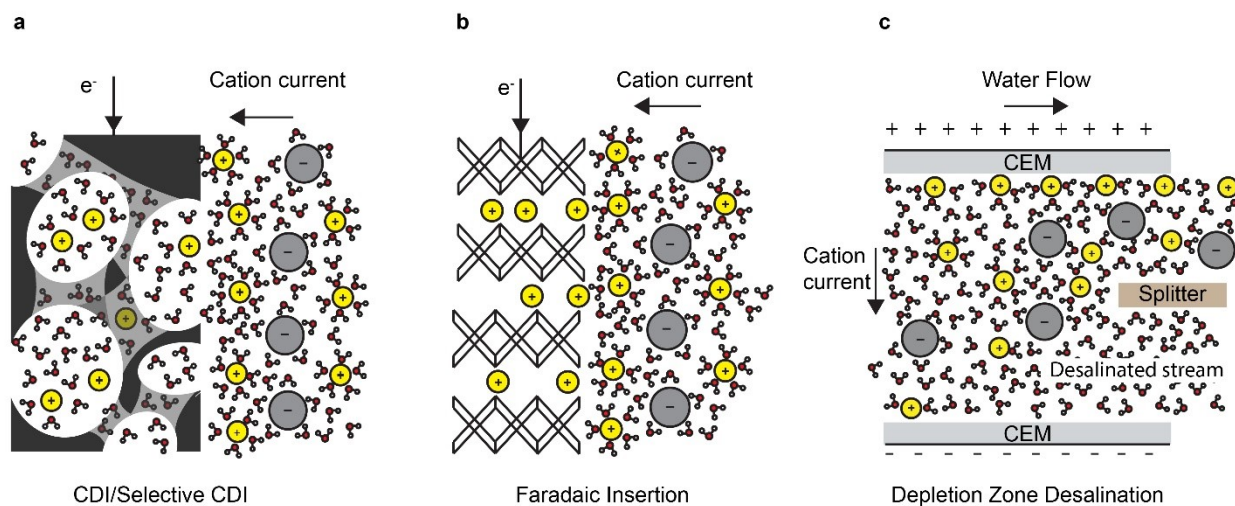

Fig. 1: Electrochemically mediated deionization mechanisms (a) Capacitive immobilization of ions in the electrical double layer. (b) Faradaic mediated intercalation of ions. (c) Deionization "shock" or depletion zone mediated ion immobilization in porous media.

By using the bulk of the electrode material, instead of just the surface (as is the case for CDI), the total capacity can be increased and efficiency in highly concentrated feed solutions can be improved[27]. The desalination battery was the first *faradaic* intercalation desalination system (Fig. 1b). Since the invention of the desalination battery in 2012[28], researchers have identified novel insertion electrode materials based on three main criteria: electrochemical stability of the electrode and the surrounding electrolyte; chemical and mechanical robustness; and the size of the interstitial sites and the insertion pathways. Several novel high-performing faradaic desalination processes such as HCDI[27], cation insertion desalination (CID)[29] and redox flow desalination[30] have since been developed.

Beyond capacitive and Faradaic ion immobilization mechanisms, depletion zone desalination, e.g. shock electrodialysis (SED)[31], is an alternative technology examined in this review for its potential to treat ion-contaminated water. Depletion zone desalination relies on a deionized region that forms at the boundary of an ion-selective element when an overlimiting current is driven through that element (Fig. 1c)[31]. The mechanisms of this process are covered in detail in Section 4 of this review.

Electrochemical deionization processes have found many applications in selective electrosorption/electrodeposition of ions, such as remediation of toxic ions from contaminated freshwater and resource mining from seawater. Tailored electrode coatings have been especially instrumental in advancing the field of selective electrosorption; researchers have used electroactive polymers, chelating polymers and redox-active polymers (conjugated and pendant-bearing) to coat electrodes for high capacity, highly selective separations[32,33]. Some prominent examples of the latter include uranium extraction from seawater[34] and chromium/arsenic oxyanion removal[35] from wastewater. Such electrode modifications coupled with modulated electric field techniques have resulted in further enhanced selectivity. The mechanisms of this process, while capacitive/pseudocapacitive in nature (Fig. 1a), are covered in more detail in Section 5 of this review.

It is important, for further development of electrochemical deionization, that there be standardization of experimental conditions and consistent reporting of performance metrics. Considering the vast amounts of capital resources and time currently being dedicated to the development of new electrode materials, cell architectures and novel selective chemistries, this field only stands to gain popularity in the future. This review aims to highlight the key methods, developments, and future opportunities in prominent electrochemical deionization methods.

2. Capacitive Deionization

CDI is an electrochemical technique employing high-surface area, conductive materials that adsorb ions from saline water. In a CDI system, two electrodes are submerged in an electrolyte; on the application of a voltage bias between the electrodes, cations migrate towards the negatively charged cathode and anions

towards the anode, where the ions are stored in the electrical double layer formed at the liquid-solid interface, effectively desalinating the feed solution. Once saturated with ions, the electrodes are short circuited or a reverse bias is applied, discharging the stored ions into a brine stream and regenerating the electrodes[16,36]. The relative advantages of CDI are detailed in Table 2, but in short, CDI is particularly energy efficient at low salt concentrations; it is characterized by fast adsorption rates, but relatively low salt adsorption capacities compared to Faradaic insertion (see Fig. 8).

2.1 CDI Performance Metrics

A single metric quantifying CDI effectiveness can vary with many system parameters, and optimization of one metric often occurs at the detriment of another. In order to accurately describe a given system's CDI performance, multiple metrics must be reported in tandem. As we outline below, reporting a rate vs. capacity diagram[37] and specific energy efficiency, allows new research to be easily comparable to existing literature (which often just report rate and/or capacity), while providing a thorough assessment of performance. Additionally, recent research on CDI metrics demonstrates that reporting the salt removal fraction (calculated from the concentration ratio of the deionized permeate to the saline feed solutions) along with energy efficiency at standardized testing conditions provides direct system-level information on how the CDI device will perform in practice[38]. Given that performance is highly dependent on test conditions (e.g. feed concentration, as shown in Fig. 8c), experiment parameters should be standardized and always reported in full.

Researchers often quote the *charge capacitance* of electrodes, easily calculable from cyclic voltammetry curves[39], which is an appropriate metric only if the *charge efficiency*—i.e. number of electrons exchanged per ion adsorbed—is also provided[40]. If the charge efficiency is omitted, the quoted performance could be artificially high due to co-ion expulsion from the electrode. More appropriate measures of electrode performance are the *energy efficiency* with which a system operates, the *rate* at which salt is removed from the feed solution and the *amount* (capacity) of salt that can be removed in a single charging step. High performance for one parameter often comes at the cost of another, so all three should be reported in tandem.

The total *specific energy consumption* (SEC) is commonly quoted in kWh m^{-3} (energy cost per volume of desalinated product) or J mg^{-1} (energy cost per mass of salt removed). The former is used frequently in reverse osmosis systems but the latter is more relevant for CDI research, where the permeate concentration varies from experiment to experiment[36]. Given that the energy required for a given separation process depends on the feed concentration, brine concentration, permeate concentration and water recovery, SEC must be paired with these parameters, or normalized by the theoretical minimum energy cost, for this metric to be meaningful[41]. Furthermore, a direct tradeoff exists between SEC—often quoted as its inverse, *specific energy efficiency* (SEC^{-1})—and deionization rate[41] (Fig. 2a), so these parameters should reported in tandem. The rate of salt removal is typically recorded as the *average salt adsorption rate* (ASAR) of an electrode: the total mass of salt adsorbed, normalized by the sampling interval and the combined mass of the cathode and anode (commonly quoted in units of mg g^{-1} s^{-1}). ASAR reported together with the *salt adsorption capacity* (SAC), commonly quoted in units of mg g^{-1}, accurately quantifies electrode performance given no efficiency constraints[37]. "ASAR vs. SAC" plots, shown in Fig. 2b and c, have been employed by many

publications in the CDI field[36,41,42]. Other practical performance metrics are CDI cycling stability, anti-fouling capability, water recovery percentage and round-trip efficiency/energy recovery[43].
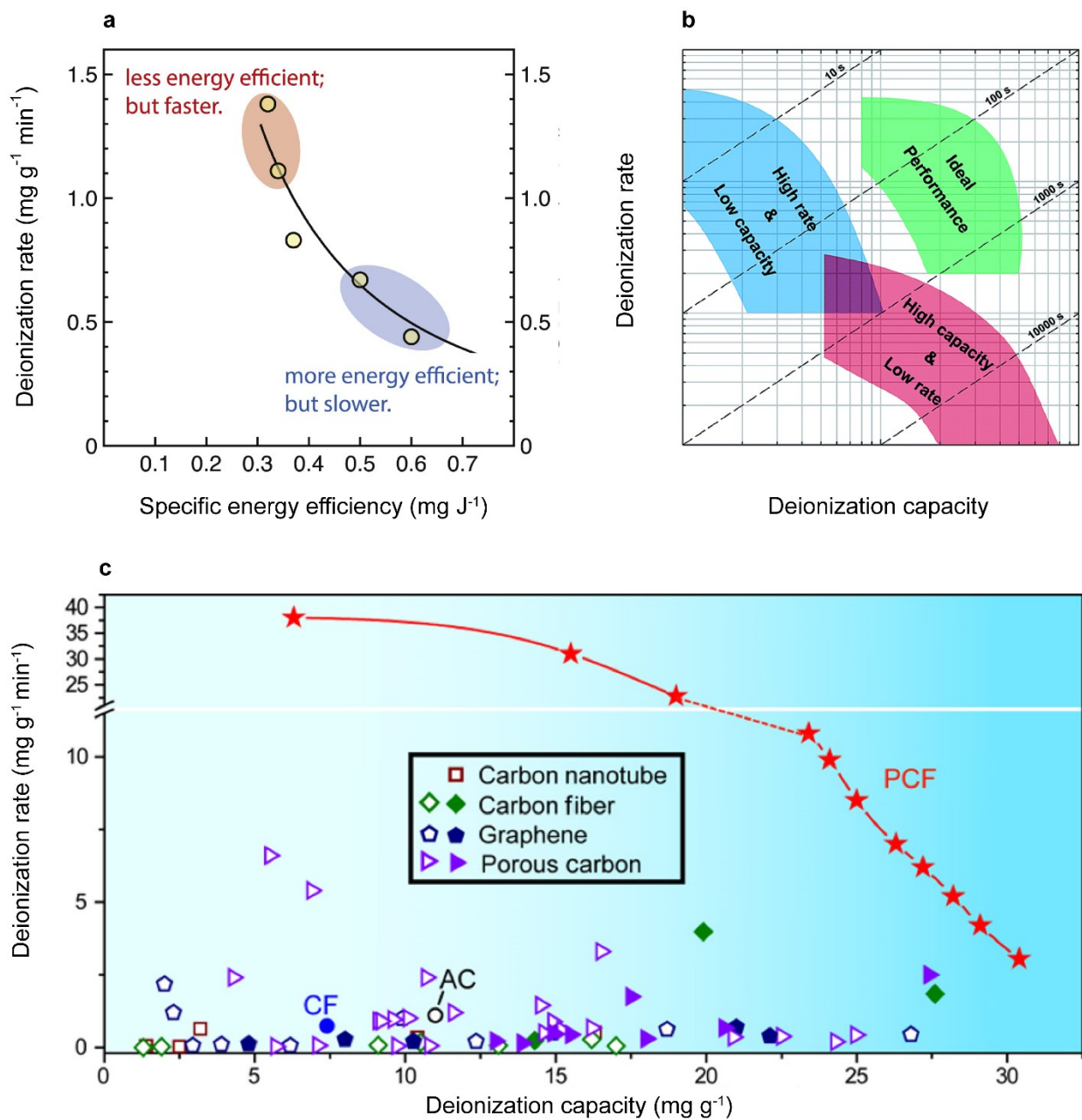
a

b

c

Fig. 2: (a) ASAR vs. SEC^{-1} plot showing the trade-off between energy efficiency and rate. Both experimental and simulated data are depicted[42]. Reproduced with permission from ref. 42. Copyright 2018 Elsevier. (b) ASAR vs. SAC (rate vs capacity) plot for generic electrodes, showing the trade-off between parameters. Dashed lines represent the time required for complete charging[37]. Reproduced with permission from ref. 37. Copyright 2014 Royal Society of Chemistry. (c) Rate vs capacity plot for recently developed mesoporous block copolymer electrodes (described in detail in Section 2.2). In showing the entirety of this rate vs. capacity plot, instead of a single point, the higher performance of this block copolymer electrode is definitively established. References for data displayed in this plot can be found in the original study[44]. Reproduced with permission from ref. 44. Copyright 2020 AAAS.

2.2 CDI Electrode Materials

The majority of CDI systems incorporate carbon electrodes given their intrinsic conductivity, high porosity and low cost[45]. Other classes of electrode materials for CDI include metal-oxides, metal-oxide carbon composites, and polymer carbon or polymer metal-oxide composites. In the following, we outline only carbon-based and two-dimensional materials, referring the reader to existing reviews on metal oxide and composite polymer materials[45,46]. To compare electrode materials described in this Section, we rely on ASAR vs. SAC diagrams due to their broad adoption and direct relevance to CDI performance; see Fig. 8a for a performance summary of existing CDI electrodes.

Activated carbon

Activated carbon, defined by its high surface area to volume ratio, was used in the first CDI system[16] developed in the 1960's; in recent years this material has been modified to achieve even higher surface areas and hierarchical pore geometries with fast charge transfer and ion diffusion kinetics. In general, activated carbon, comprised of aggregates of microporous particles, is fabricated through pyrolysis of a carbon precursor, such as wood, then is activated (i.e. micropores are created) via chemical etching or gasification of the product[45]. Although the typical performance of activated carbon electrodes does not

match those of 1D and 2D materials (see Fig. 8a for a comparison), the low cost of activated carbon makes it an appealing electrode material for commercial applications[47,48].

Examples of modifications to activated carbon include the addition of carbon black with a polymeric binder (more than doubling total salt removal without changing system conditions)[49], KOH etching and CO_2 gasification of coconut shell-based activated carbon to tune the pore size distribution; an increased density of micropores led to enhanced SAC relative to most other activated carbon electrodes[47]. By tuning the pore size distribution of activated carbon synthesized by the template method, a subsequent study measured a slightly larger SAC[50]. An increased SAC (~ a factor of two over bare activated carbon) and CDI performance was also observed in reduced graphene-oxide activated carbon composites[51]. In these electrodes, the graphene oxide acts as a bridge between activated carbon particles, simultaneously preventing restacking—increasing specific surface area—and enhancing electrode conductivity. Employing doped activated carbon electrodes in an asymmetric CDI cell has proven an effective method to enhance the SAC, while still employing relatively low-cost materials, as in a p-toluenesulfonate doped carbonized polyanaline electrode[52], and more recently a N-doped activated carbon electrode (see Fig. 8a)[53].

Carbon aerogels

Carbon aerogels are in many ways the ideal material for capacitive deionization systems. This intrinsically conductive foam has a monolithic mesoporous structure (as opposed to the particulate structure of activated carbon), leading fast ion diffusion kinetics (ions can easily diffuse through the mesoporous structure) while retaining high adsorption capacity[54]. Like activated carbon, carbon aerogels have a high specific surface area, low thermal expansion coefficient and are highly chemically resistant[45]. The first application of an aerogel applied for CDI came from Lawrence Livermore National Laboratory in 1996[18], after which many follow up experiments improved on their quoted performance by, for example, modifying the aerogel synthesis process to tune the pore size distribution[55], or adding reduced graphene oxide flakes and nanofibers to increase surface area, conductivity and prevent aggregation of particles[56, 57]. In one of these studies, an aerogel with graphene oxide sheets interconnected by polyacrylonitrile nanofibers was

synthesized and tested for CDI performance, resulting in high rate and capacity, while remaining stable for over 100 cycles[57]. Recently the specific ion adsorption capacity for carbon aerogels was pushed even further by maximizing the density pores in the 2-5 nm range and enhancing the wettability and conductivity of the electrode via N-doping[58] (see Fig. 8a for performance data).

Two-dimensional materials

Graphene and graphene-like materials have large specific surface areas and high conductivity; they are consequently promising candidates for CDI electrodes. Graphene, exfoliated via the Hummer's method and dip-coated on carbon substrates has the advantage of high specific area (a maximum of 222 $m^2 g^{-1}$ while retaining high conductivity)[59]. The first study using graphene as an electrode was hindered by restacking of graphene nanoflakes, achieving a specific surface area of only 14.2 $m^2 g^{-1}$ (less than 7% of the maximum theoretical value), but still showed decent electrosorptive performance, with a SAC of 1.85 mg g^{-1} [59]. In a follow up study, the same group improved the electrode performance by increasing amount of nitric acid used in the first step of the Hummer's method, thereby increasing the specific area to its maximum value[60].

To further improve the performance of graphene electrodes, several groups prepared three-dimensional graphene structures by using sponge[61] or polysterene[39] templates, increasing the accessible surface area. In the former, the specific surface area reached 305 $m^2 g^{-1}$ leading to greater ion adsorption capacity of 4.95 mg g^{-1} for a 0.5 M NaCl solution. The total electrosorption capacity of graphene-based electrodes was pushed beyond that of activated carbon and carbon aerogels by increasing the frequency of defects in the graphene sheets, which effectively increases the density of micropores and dramatically increases the ion adsorption capacity (see Fig. 8a)[62,63].

The performance of graphene CDI electrodes was also enhanced via the addition of carbon nanotubes to graphene oxide sheets. The composite demonstrated higher conductivity and porosity relative to pure graphene oxide electrodes; the study reported high adsorption capacity (Fig. 8a), a 98% salt removal efficiency of 1500 ppm NaCl solution, all with low energy requirements (0.8 kWh m^{-3})[64]. Recently, two-dimensional materials beyond graphene have captured significant interest for a variety of applications, from

semiconductors to catalysts and membranes; examples include MXenes[65,66] and MoS$_2$/graphene[67] composite materials. One of these materials, molybdenum disulfide chemically exfoliated in its metallic 1T phase, was shown to act as high-performing CDI electrode[68]. By increasing the frequency of defect sites by thermally treating flower-like MoS$_2$, the specific capacity was increased nearly threefold, approaching the capacity of the highest-performing graphene-based CDI electrodes, and surpassing that of carbon aerogels and activated carbon (see Fig. 8a).

Mesoporous carbon

In addition to the categories listed above, a broad class of materials generally deemed *mesoporous carbon*, which can be synthesized through a wide variety of techniques including sol-gel synthesis and direct carbonization of polymer structures or metal organic frameworks, show high CDI performance[55,69,70]. One example of mesoporous carbon, synthesized via self-assembly of a tri-block copolymer, was compared directly to a carbon aerogel. The former demonstrated a greater than threefold capacity increase relative to the latter (tested under the same conditions)[71]. Subsequently, an even higher capacity of 20.63 mg g^{-1} in ~500 mg L^{-1} NaCl solution was measured in nitrogen-doped mesostructured nanocrystals[72]. In two recent advancements, the highest capacities of any electrode material for CDI was measured in two separate hierarchical carbon structures with a high density of both meso and micro pores (see Fig. 8a)[44,73]. Despite similarly high performance, the two structures were fabricated with entirely different procedures: one *via* self-assembly of block copolymer fibers and the other *via* calcination of biomass with an activator to create micropores.

2.3 CDI Systems

Several CDI architectures have been developed, each of which have their unique tradeoffs, as described in Table 1. As a significant portion of CDI research focuses on electrode material (as opposed to system-level innovation) and CDI technology remains in the research phase, the simplest systems – flow-between CDI and membrane CDI – are the default. Flow electrode CDI, invented only recently, shows great promise as a new technique that transcends the capacity limitations of more standard configurations.

CDI Configurations	Advantages	Disadvantages
Flow-between	• Simple and economical • High water flow rate possible (water does not pass through any active element) • Isolates electrode characteristics – useful for fundamental studies	• Co-ion expulsion leads to reduced capacity and efficiency • Diffusion-limited desalination (incomplete desalination for large volumes or flow rates)
Membrane CDI	• Co-ion expulsion eliminated • High water flow rate possible • Tailored ion-selective separation possible with existing technology	• High cost of ion-selective membrane • Diffusion limited desalination
Flow-through CDI	• Close contact of feed with electrode at all points (fast adsorption rates)	• Fouling is a concern • Water flow rate is limited by the pore size distribution of the electrode • Ion selective membrane is difficult to adopt due to water flux constraints
Flow-electrode CDI	• Continuous desalination possible (no pause for desorption step needed). • Effective capacity (mass of salt removed, normalized by the contact area between the feed solution and electrode compartment) can be increased simply by increasing electrode flow rate	• Complicated implementation with limited architectures (flow-through not feasible). • Electrode must be "flowable", limiting material choice.

Table 1: Comparison of the four dominant CDI systems.

Flow-between CDI

In the first CDI cell design[16], which has been employed by many subsequent studies[17,18], two electrodes are placed parallel to each other in an electrolyte. Saline water flows in the space between the electrodes in a "flow-between" geometry. This design has the advantage of simplicity, low cost, and relatively little propensity for fouling[36] and is used for many fundamental studies on electrode properties[47,57].

Membrane CDI

In a typical CDI setup, the ionic current at the electrode-solution interface can be carried by counter-ion adsorption or co-ion expulsion. Co-ion expulsion adds ions *back to* the solution from the electrode, reducing the effective deionization rate. MCDI increases charge efficiency by eliminating the possibility of co-ion expulsion through placement of ion-exchange membranes (IEMs) on one or both electrodes[74]. In a direct comparison between CDI and MCDI (tested with graphite cloth electrodes and commercial membranes), the latter displayed an increased SAC and SEC for a range of applied voltages and feed concentrations. (E.g. for biases of 2.0 and 3.5 V, the SAC for CDI was 3.0 and 3.5 mg g^{-1}, respectively; these metrics increased to 4.0 and 7.5 mg g^{-1} for MCDI). We refer the reader to a detailed review on the benefits of MCDI over CDI desalination for more details concerning this important development[40,75]. Researchers have also directly treated the electrodes used in an MCDI cell for counterion selectivity. Carbon electrodes treated with the cation exchange coating sulfosuccinic acid (SSA) crosslinked poly(vinyl alcohol) (PVA) demonstrate increased charge capacitance and SEC by 27-56% compared to uncoated electrodes[20]. The increased current efficiency in this study is attributed to the selective transport of ions between the electrode surface and bulk solution courtesy of the ion-exchange polymer[20,76]. MCDI can also lead to targeted, selective ion adsorption, as shown in Fig. 3a [77] and described in detail later in this Section and in Section 5.
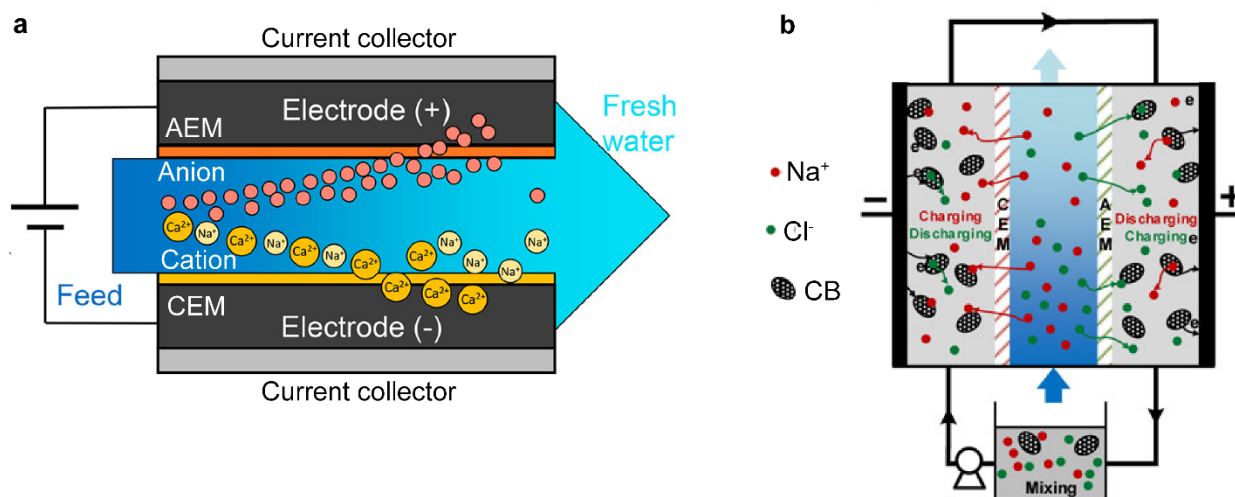
Fig. 3: (a) Example of MCDI applied to selective removal of divalent cations[77]. This setup is in the "flow-between" geometry, as is standard for MCDI systems. Reproduced with permission from ref. 77. Copyright 2019 American Chemical Society. (b) An FCDI setup, wherein not only the feed solution, but the electrodes themselves, are continuously replenished. In this work, the electrodes are cycled from one half-cell to the other to allow continuous reuse of the active material[78]. Reproduced with permission from ref. 78. Copyright 2020 American Chemical Society.

Flow-through CDI

The "flow-through" geometry was invented in 1970[79], soon after the standard flow along geometry. In the former, saline water flows parallel to the electric field, through the electrodes and normal to their surface. This system can obtain faster adsorption rates and benefits from a lower cell resistance than in the standard flow along geometry[36]. In the flow-along geometry, the volumetric flow rate depends on the spacing between electrodes, with larger electrode-gaps leading to larger flow rates; in flow-through geometries, however, this space can be minimized (reducing the potential drop from the finite electrolyte resistance and reducing ion diffusion time) without affecting volumetric flow[80]. As shown in recent work, the reduced ion diffusion time can dramatically increase the ASAR by roughly 4 to 10 times—this work cites an improvement from 0.25 mg g^{-1} min^{-1} to 0.96 mg g^{-1} min^{-1}— while retaining a high (at a maximum 10.2 mg g^{-1}) SAC[80]. It should be noted that a more dilute feed solution was tested in this work. These benefits come at a cost, however, as flow-through electrodes must have a more complicated pore-size distribution to accommodate both bulk flow and ion uptake; the water flow rate is limited by the size of the electrode pores. Additionally, the electrode has a higher propensity for fouling than its flow-along counter-part[36].

Flow-electrode CDI

In a recent addition to the set of CDI systems, flow-electrode capacitive deionization (FCDI) was invented to solve the persistent issue of the finite adsorption capacity of standard CDI cell designs[81]. In FCDI, a carbon slurry flows through channels between the current collector and IEM, continuously replenishing the

capacitive material and eliminating the need for the regeneration step that pauses desalination (Fig. 3b). Various closed-systems, in which the slurry is continuously discharged and re-used without pausing the desalting step, have been demonstrated[82,83]. Because the electrode material is continuously regenerated at a rate set by the electrode flow speed, performance metrics such as electrode capacity become less important; the limiting factor for FCDI, as shown in recent studies, is instead electrode conductivity.

In a typical FCDI electrode, where a mixture of activated carbon and a carbon black is used, the conductivity is only 0.1 -1 mS cm^{-1}, several orders of magnitude lower than conventional CDI electrodes[84]. By sacrificing SAC for electrical conductivity (using only carbon black as the electrode material) a recent study demonstrated enhanced ASAR, scaled by the membrane area, by a factor of five[78]. Consequently, the total salt removal increased without any decrease in energy efficiency. The absolute value of energy efficiency reported in this same study, $\sim$ 8 μmol J^{-1}, is on the same order of magnitude as that of a standard MCDI system[41], but we remind the reader that such comparisons are ambiguous at best (see Section on CDI metrics).

2.4 CDI Theory

Over the past two decades, accurate and tractable models describing CDI have been developed, the bulk of which rely on a sophisticated theoretical understanding of the electrical double layer in porous structures on multiple length scales[85]. The usual model system is comprised of an aqueous electrolyte solution embedded in a conductive porous electrode. In non-faradaic CDI, charge is stored exclusively in the electrical double layer (EDL) at the interface of the electrode and electrolyte in the form of adsorbed ions. The classical description of the EDL, which is applicable for mesoporous structures or highly concentrated electrolytes, is the Guoy-Chapman-Stern (GCS) model. Here, the EDL is composed of the Stern layer—a fixed capacity region at the electrode surface stemming from the finite size of adsorbed ions—and a diffuse region with a mixture of co-ions and counterions[86,87].

The GCS model system applies for both CDI electrodes and supercapacitors, with a few crucial differences: in the former, the bulk electrolyte concentration changes appreciably with time (whereas for supercapacitors

a negligible fraction of the ions from the bulk solution are adsorbed). Further, the ratio of counterion adsorption and co-ion expulsion is, for CDI, both important (whereas for supercapacitors only the overall charge matters) and, in useful systems, always >1. As a result, the standard transmission line model (an RC circuit where the ionic resistance of the electrolyte is added in series to the capacitance of the EDL) used to describe supercapacitors and the original CDI systems[88], fail to describe CDI behavior[86]. The GCS model has been used to describe systems in which the EDL is small compared to the size of the pores; it parameterizes the Nernst-Planck equations describing ion adsorption dynamics for a range of applied voltages and feed concentrations[87].

When the Debye length is larger than the size of the electrode micropores (<2 nm in diameter), the GCS model breaks down[89]. The EDL, instead of being a smooth layer on a flat or gently curving surface, has discontinuities at the location of micropores, where the EDL on the sides of the pores overlap. To account for these discontinuities, the modified Donnan (mD) model was developed. The mD model is an extension of the Donnan model[90,91], which assumes complete overlap of the Debye layer within pores, thereby creating a step-function potential over the porous electrode surface. The mD model adds two important factors: first, it includes the Stern layer at the pore surface; second, it adds an attractive chemical potential in order to describe data showing salt adsorption in microporous structures without an applied voltage[14]. The ion concentration in micropores can then be described according to the Boltzmann equilibrium relation.

The mD model was further improved by allowing the chemical potential term to vary with the micropore salt concentration, thereby eliminating the prediction of unrealistically large adsorption capacities at high salt concentrations[14]. It has also been extended from the one-dimensional case to cell-level, two-dimensional systems[92], and has been corroborated by molecular dynamic simulations[93]. The mD model was applied to describe a series of CDI developments such as "inverted CDI" by fixing charge in the micropores to emulate chemical treatment[15], inclusion of surface transport[94] and an explanation of the benefits of pulsed-flow CDI over continuous flow systems[95].

Directly consequential for materials design, the mD model incorporates – although it fails to fully explain— the effect of micropores on electrode capacity through the non-electrostatic potential term. The effect of micropores on CDI performance has been subsequently quantified through the fitting of pore size distributions[96], with the strict condition that capacity increases as micropore fraction increases, but decreases as mesopore fraction increases. (It is important to note that although capacity may suffer with increasing mesoporosity, adsorption rate will benefit from the increased density of ion pathways in the electrode[96]). As shown in Fig. 4, this guided fitting procedure leads to an accurate predictor of electrode capacity. The importance of micropore fraction in electrode capacitance has been corroborated repeatedly and is a standard guideline for electrode materials design[97].
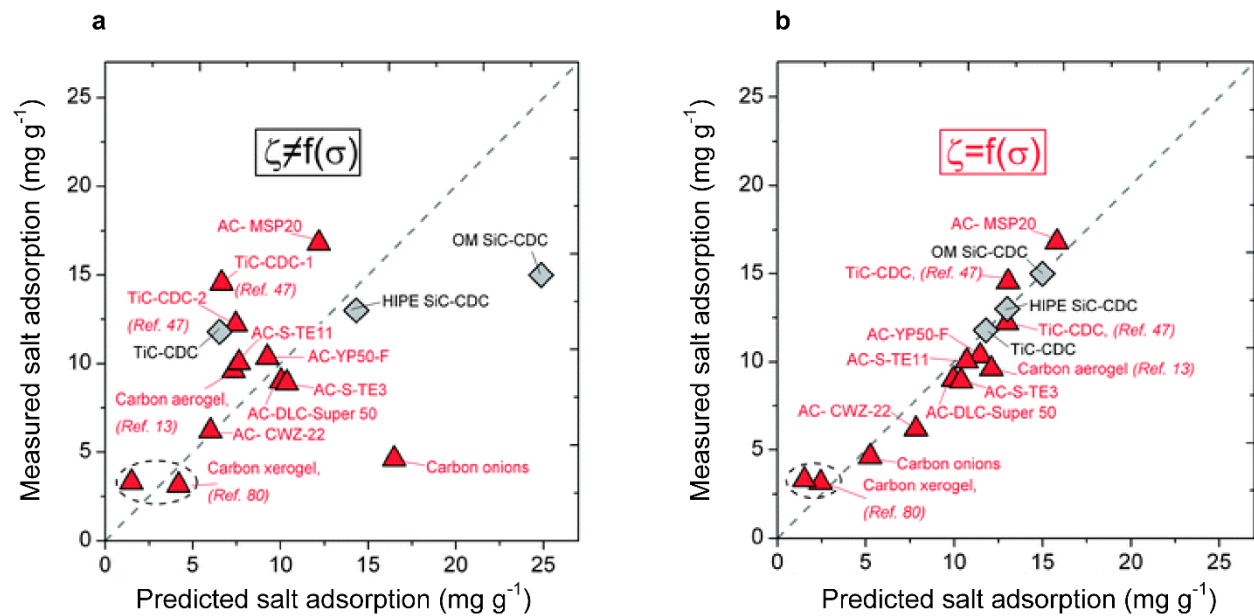

Fig. 4: (a) Adsorption capacities predicted through an empirically based model without consideration of pore size distribution. No relationship between predicted and measured adsorption capacity is observed. (b) Adsorption capacity predicted through empirical model considering only the pore size distribution, leading to a one-to-one correspondence between predicted and measured values[96]. This work displayed the importance of the pore size *distribution*, over just frequency of pores, in determining adsorption capacity. Reproduced with permission from ref. 96. Copyright 2013 American Chemical Society.

19

Recently, a simplified approach based on the Langmuir isotherm (as opposed to a physics-based description of the EDL) has been developed and named the dynamic Langmuir isotherm[98]. The use of the Langmuir isotherm has been criticized in existing reviews[9,36], which claim that the underlying physics are based on the adsorption of uncharged gasses, and as such cannot incorporate the effects of co-ion expulsion (charge efficiency), asymmetric electrodes, or voltage dependence.

The dynamic Langmuir isotherm accounts for these factors, however, as well as ion composition; the model accurately fits experimental CDI data, taken under a range of experimental conditions. A major benefit of this model is that it can describe and predict, among other things, selective adsorption from mixed ion solutions for all possible ion combinations[99]. However, because the model omits the details of electrode structure or material, it must be calibrated for each new material used, a drawback that will surely limit the applicability of this theoretical development.

2.5 Selective CDI

The selective capabilities of pristine carbon surfaces in CDI cells have been demonstrated in several studies involving lithium[100,101], nitrate[24–26,102] and fluoride removal[103]. In general, two factors intrinsic to all CDI processes affect selectivity of one ion over another: steric hindrance and electrostatic attraction. These two effects often work in opposition to each other: for small pore sizes, the diffusion of large and multi-valent ions is hindered, giving rise to selectivity towards monovalent ions[22,104]; multivalent ions, however, experience a larger attraction to the charged electrode surface, leading to displacement of monovalent ions with multivalent species[105].

Depending on the application, selectivity towards monovalent or multivalent ions is preferred. Relying only on the steric effects of micropores, and without employing an IEM or functionalizing electrode surfaces, monovalent ions are typically selectively adsorbed. In one study[22], researchers pursued selectivity towards monovalent ions by continuously tuning the pore size of activated carbon via chemical vapor deposition. At pore diameters falling between the hydrated radii of alkaline earth cations such as Ca^{2+} and Mg^{2+} and

that of monovalent cations such as Na^+, electrodes only adsorbed the monovalent ions, leaving the divalent cations in solution. Size selectivity was also employed to demonstrate selective removal of nitrates over chloride and sulfates in feed solutions, as the nitrate ion is only weekly hydrated[23].

Covered in great detail in Section 5, coatings and membranes can be applied to electrode surfaces in order to induce selectivity, as opposed to relying on selectivity intrinsic to the electrode material[77]. For example, a recent study employed a cation exchange membrane in an FCDI system to selectively remove Ca^{2+} over Na^+ with applications in water softening. This study demonstrated 6-fold selectivity of Ca^{2+} over Na^+ at low (10 mA m^{-2}) current densities in a 2000 mg L^{-1} NaCl and 150 mg L^{-1} CaCl$_2$ solution. Energy consumption was only 0.44 kWh to achieve an effluent salinity of 500 mg L^{-1} and Ca^{2+} concentration of 15 mg L^{-1}.

3. Faradaic Desalination

Electrochemically driven desalination based on Faradaic reactions has been a growing field of study since the creation of the desalination battery by Pasta *et al.* in 2012[28]. The desalination battery system is like CDI, only charge is stored in chemical bonds in the bulk of the electrode material instead of the electric double layer on the surface of the material. Ion storage occurs through insertion of the ion into a lattice site of a host crystal structure coupled with a redox reaction of an element contained in the host. The low fixed voltages for driving the insertion mechanism results in a low energy input system. Also, insertion materials have high specific capacities for ion removal, but have a slower ion removal rate compared to standard CDI for desalination[106,107]. Faradaic desalination performance has been summarized in Fig. 8b, Fig. S1, and Table 2S. These electrode materials also greatly benefit from the vast amount of research in energy storage, especially the development of aqueous Na-ion batteries, which are governed by the same parameters[108–110].

3.1 Materials

Extensive research into energy storage materials has elucidated a set of constraints for batteries used in aqueous electrolytes; these constraints transfer directly to desalination batteries. First, the operating potential of the material must fall within the redox potential window of the electrolyte. In the case of aqueous electrolyte, the window is set by the evolution potentials of H_2 and O_2 via electrochemical water

splitting[111,112]. Electrode materials that meet this constraint, along with the pH dependence of the aqueous redox potential, are shown in Fig. 5 [108]. Second, aqueous battery materials must be chemically stable in the given pH of the aqueous electrolyte and must avoid electrode dissolution and side reactions with dissolved O_2 [112]. Third, materials must have interstitial sites and migration pathways that are large enough to allow ion storage while minimizing volume change during cycling[113–115].

Na-ion battery electrodes used for desalination of aqueous NaCl solutions include different phases of Na_xMnO_2 (NMO) [28,116–118], $Na_2FeP_2O_7$ [119,120], NASICON-type $Na_3V_2(PO_4)_3$ [121,122], NASICON-type $NaTi_2(PO_4)_3$ (NTP) [123,124], and Prussian blue and its analogues[125–128]. The mechanisms for Cl⁻ capture include conversion reactions with silver/silver chloride and bismuth/bismuth oxychloride[28,123,129]; oxidation of Cl⁻ to form chloride species (Cl_2, HOCl, radical Cl)[130]; and intercalation into MXenes, which can host a wide range of cations and anions[131–133].
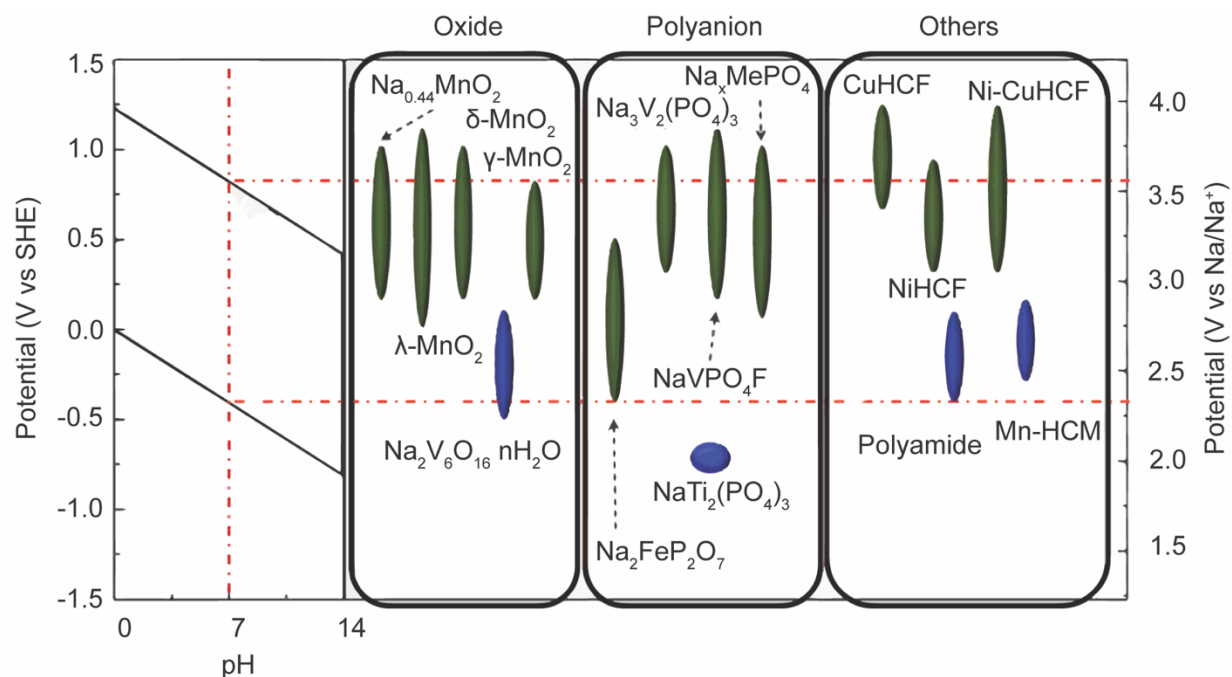

Fig. 5: Electrode material operating potentials vs SHE and Na/Na⁺. The red dotted line indicates the H_2 and O_2 evolution limits at neutral pH. The leftmost inset shows the evolution voltage limits as a function of pH. Reproduced with permission from ref. 108. Copyright 2014 American Chemical Society.

3.2 Desalination batteries

The first desalination battery in 2012 used $Na_2Mn_5O_{10}$ (NMO) nanorods for Na^+ removal and Ag for Cl^- removal, demonstrating membrane-free desalination with battery materials[28]. As shown in Fig. 6a, desalination follows a four-step process. The electrode selectivity for intercalation of Na^+ in NMO and reaction of Cl^- with Ag prevent the co-ion expulsion effect; an ion selective membrane is therefore not necessary. This process required 0.29 kWh m^{-3} for 25% salt removal, approaching the reverse osmosis energy requirement of 0.20 kWh m^{-3} for similar conditions. The key limitations were the low NMO electrode capacity of 35 mAh g^{-1} relative to the average capacity of 160 mAh g^{-1} of Li-intercalation electrodes, the high cost of Ag, and the kinetic limitations of AgCl due to its poor electronic conductivity[28].
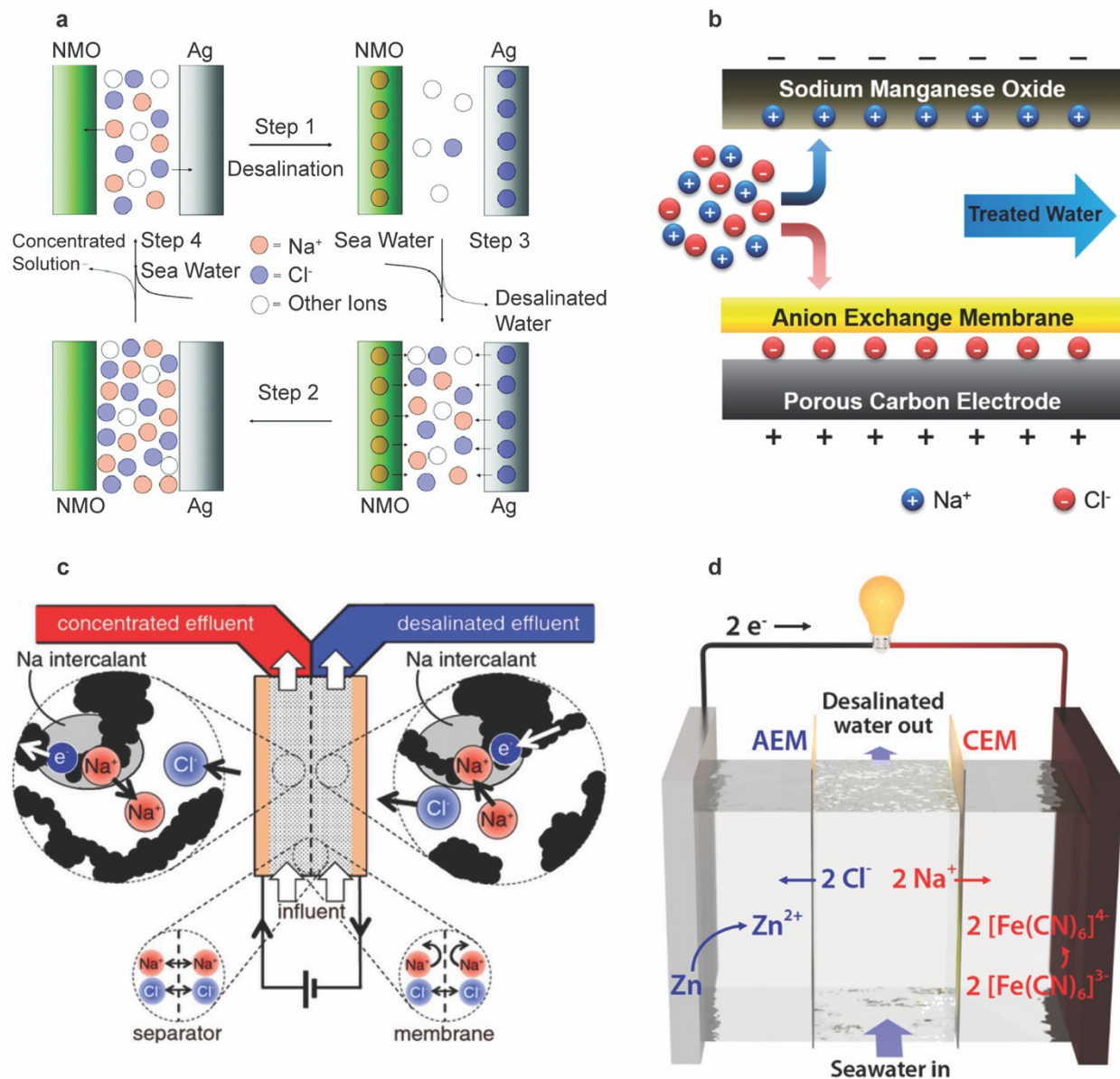
Fig. 6: (a) Schematic representation of the complete cycle of the desalination battery. Reproduced with permission from ref. 28. Copyright 2012 American Chemical Society. (b) Schematic of HCDI during the desalination process. Reproduced with permission from ref. 118. Copyright 2014 Royal Society of Chemistry. (c) Schematic of the symmetric CID cell during desalination of the right stream and concentration of the left stream. Reproduced with permission from ref. 29. Copyright 2016 The Electrochemical Society. (d) Schematic of the flow battery desalination cell during the desalination process. Reproduced with permission from ref. 30. Copyright 2018 American Chemical Society.

The promising results of this seminal study have motivated further research of intercalation materials for desalination batteries, focused mainly on development of high capacity Na-intercalating electrodes and alternatives for the Ag electrode. A potential alternative to Ag electrodes for Cl^- storage, bismuth electrodes exploit the conversion of Bi to $BiOCl$[123]. The primary motivation for this alternative is its lower cost [134,135]. Unfortunately, Bi electrodes suffer from H^+ production during oxidation of Bi to BiOCl, which lowers the solution pH, and slow kinetics of the reduction reaction converting BiOCl to Bi in non-acidic conditions. The Na^+ removal was performed with a NASICON-type $NaTi_2(PO_4)_3$ electrode due to its high theoretical capacity. This electrode paring with Bi removes 3 Na^+ for every Cl^-, which decreases the pH. Due to the imbalance of the ion removal and the decreasing pH, the $NaTi_2(PO_4)_3$ was replaced with a Pt electrode in a second deionization step to reduce the H^+ ions to H_2 while the remaining Cl^- were removed, thus neutralizing the desalinated water. A salination step must be performed in a waste stream to regenerate the original electrode structures. $NaTi_2(PO_4)_3$ will spontaneously oxidize in acidic conditions, however. To prevent this, a Nafion membrane was added to protect the Na-electrode from the acidic electrolyte required to lower the kinetics for the BiOCl reduction.

With a 0.6 M NaCl feed solution, the process required 5.9 kWh m^{-3} for removal of 21.23 g of Cl^-, a higher value than the 1.3 kWh m^{-3} required for the NMO/Ag battery under similar conditions[28]. Further research replaced NAISCON-type $NaTi_2(PO_4)_3$ with the Prussian blue analogue, $Cu_3[Fe(CN)_6]_2 \cdot nH_2O$, which is chemically stable in acidic conditions but has a lower capacity[136]. This electrode change allows for a membrane-free desalination and salination process with an energy cost increase. The increase originates in the voltage difference between the two electrodes where the NAISCON-type electrode has nonspontaneous desalination and spontaneous salination while the Prussian blue analogue has spontaneous desalination and nonspontaneous salination when coupled with the Bi electrode.

For the desalination of brackish feed solution, a different design included both a cation selective membrane (CEM) and anion selective membrane (AEM), creating a three-stream system. The two streams at the electrode interfaces are held at higher concentration than the feed. This cell architecture increases the mass

25

transfer limit at the electrode-electrolyte interface, which prevents kinetic limitations and improves the ion removal rate when dealing with lower concentration feed solutions[137].

3.3 Hybrid capacitive deionization

The desalination battery and CDI systems both have inherent limitations, which can be surpassed when the systems are combined. The incorporation of a Na^+ insertion electrode allows an increase of the cation storage capacity and induces cation selectivity. CDI outperforms the desalination battery design in salt removal rate, which in a desalination battery is limited by the slow kinetics of the Cl^- capture electrodes. Hybrid systems were developed by replacing one of the carbon electrodes from CDI with an insertion electrode from the desalination battery, thus combining the high rates of CDI with the large capacity and selectivity of the desalination battery. The seminal work on hybrid CDI (HCDI) incorporated a $Na_4Mn_9O_{18}$ electrode into a CDI system. In this system, $Na_4Mn_9O_{18}$ captures Na^+ via intercalation while Cl^- crosses an AEM for storage in the EDL of an activated carbon electrode (Fig. 6b)[118]. The total capacity of the system of the HCDI was much higher than their own results for CDI and MCDI tested under the same conditions. The peak ion removal rate for HCDI was higher than their results for CDI but slightly lower than MCDI tested under the same conditions. The desalination performance in this work demonstrated the benefits of HCDI and motivated further development of the system with new cathode materials.

HCDI has been successfully demonstrated using a suite of cathode materials: $Na_2FeP_2O_7$[120], Prussian Blue $Na_xFe_2(CN)_6$[127], and different phases of MnO_2[138–140]. Key results from these works include the establishment of ion removal capacity and ion removal rate relationships, identification of materials with open frameworks resulting in faster kinetics, and elucidation of phase changes due to multi-ion insertion. For establishing ion removal capacity and ion removal rate relationships, results from desalination with $Na_2FeP_2O_7$ indicate that with slower ion removal rates ion removal capacity is higher relative to MCDI (20% increased capacity at 10 mM NaCl feed solution and 50% at 100 mM NaCl feed solution)[120]. At faster ion removal rates, however, the ion removal capacity is equivalent to MCDI at 10 mM NaCl feed solution and larger by only 20% at 100 mM NaCl.

For materials with open frameworks, **Prussian Blue** $Na_xFe_2(CN)_6$ was studied for its theoretically high capacity and fast insertion kinetics[127]. Prussian blue electrodes were synthesized as nanocubes incorporated into a nanoporous, reduced graphene oxide framework (PB@NPG). PB@NPG achieves a high ion removal rate of 0.5430 mg g^{-1} s^{-1} with a capacity of 20 mg g^{-1} at a 40 C applied current. The increased capacity of PB@NPG is possibly due to the NPG protecting the PB from flowing electrolyte, which can remove particles adhered to the surface of graphene oxide. The porous electrode structure also improves the rate capabilities. PB@NPG also sustained an ion removal rate of 0.2925 mg g^{-1} s^{-1} at a capacity of 40.8 mg g^{-1} for 600 cycles at a 20 C applied current. The incorporation of insertion electrodes into porous structures enables improvements of both capacity and rate[141].

For investigating the phase changes resulting from multi-cation insertion, layered manganese oxides containing hydrated cations were employed in an HCDI system. These structures included Na-birnessite and Mg-buserite in solutions of NaCl and $MgCl_2$ [140]. The structure and phase transformations of insertion electrodes due to such mixed electrolytes is relevant for HCDI systems operating in real brackish water and seawater, which can contain Na^+, K^+, Mg^{2+}, and Ca^{2+} [138,140]. Electron dispersion spectroscopy and x-ray diffraction (XRD) measurements indicate that insertion of Mg^{2+} into Na-birnessite and Na^+ into Mg-buserite is accompanied by material phase transformations. XRD measurements revealed that Mg-buserite has a lower crystallinity than Na-birnessite, which may cause poor stability in the Mg-buserite. The degree of crystallinity was determined by the full width half max of the (001) peaks and the presence of XRD peak shoulders upon cycling. From this work it is reasonable to infer that materials with higher crystallinity provide longer cycling stability. Further understanding of insertion material changes due to multi-ion insertion and its effects on desalination performance will be necessary for using Faradaic insertion desalination in real conditions.

3.4 Cation insertion desalination

Insertion electrodes have demonstrated high capacities for Na^+ removal in desalination batteries and HCDI. Taking advantage of this high capacity, Smith and Dmello proposed a symmetric cell design, currently

called cation insertion desalination (CID), and simulated the local electrochemical processes in which both electrodes are built from cation insertion material, only one is filled to capacity with Na^+ and the other is empty[29]. Inspired by the rocking-chair battery concept in Li-ion batteries, the symmetric design takes advantage of the salt depletion effect, the simultaneous accumulation and depletion of salt ions in solution at opposing electrodes[142]. As shown in Fig. 6c, Na^+ intercalates into the anode from a NaCl influent stream producing a desalinated effluent and Na^+ deintercalated from the cathode into a parallel influent stream producing a concentrated effluent that is separated by an anion selective membrane. The charge imbalance between the two streams causes Cl^- ions in the anode-side stream to diffuse across the anion selective membrane into the cathode-side stream, creating a freshwater stream and brine stream. Once the capacity of the electrodes is filled or exhausted, the effluent tanks are switched, allowing the process to continue. An NMO CID cell operating at a C/2 rate was predicted to desalinate a 700 mM NaCl solution by 63% with energy consumption of 0.74 kWh m^{-3} and 50% water recovery. The work also predicted 59-64% drop in influent salinity for 70 mM and 700 mM with water recovery levels of 95% and 80%, respectively. These optimistic simulation results have motivated additional development of porous electrode theory coupled with fluid flow and ion transport across anion selective membranes for desalination with intercalation materials[143–145].
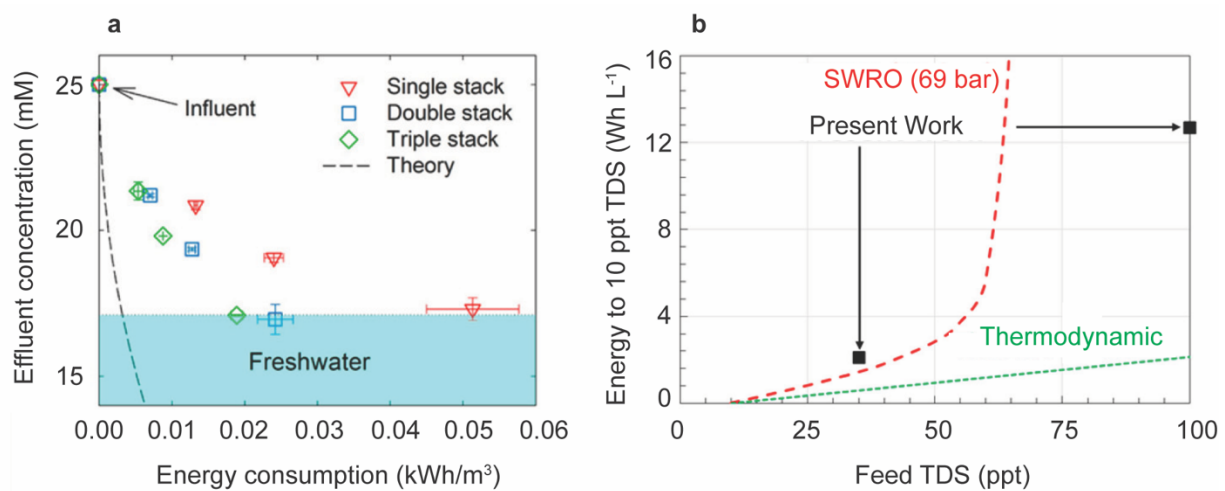
Fig. 7: (a) Energy consumption to desalinate 25 mM NaCl for single, double, and triple stacks of membranes. Reproduced with permission from ref. 146. Copyright 2017 American Chemical Society. (b) Energy consumption of redox flow battery design compared to seawater reverse osmosis (SWRO). Reproduced with permission from ref. 30. Copyright 2018 American Chemical Society

In experimental settings, the rocking chair design was implemented with two Prussian blue electrodes, NaNiHCF and NaFeHCF[147]. The Prussian blue electrodes were chosen for their higher capacity relative to that of NMO and their ability to reversibly intercalate Na^+, K^+ Mg^{2+}, and Ca^{2+} [126,148]. In seawater conditions, the Prussian blue system removed 40% of Na^+ with an energy consumption of 0.34 kWh m^{-3} and 50% water recovery. For 25% Na^+ removal, the energy consumption is 0.14 kWh m^3 which is much lower than the 0.29 kWh m^{-3} for the original desalination battery [28]. These results demonstrated high desalination capacity at a low energy cost, but further optimization is needed to approach water recovery levels of 95%, as proposed by Smith and Dmello[29]. Analogous to the CID system, an anion insertion desalination has been experimentally demonstrated with symmetric Ag/AgCl electrodes. The Ag electrode benefits from a high theoretical capacity, but has kinetic limitations, especially in brackish conditions[149].

Recent related designs have taken advantage of the salt depletion effect to lower energy consumption, improve mass-limiting current, and desalinate highly concentrated influents. Adding cation and anion selective membranes in a CID cell creates new brine streams and freshwater streams without adding additional electrodes. Scaling up the system to include at least three stacks reduces the total energy consumption (Fig. 7a). For a triple stacked cell, a brackish stream of 25 mM NaCl desalinated to 17 mM NaCl requires only 0.02 kWh m^{-3} [146].

3.5 Redox flow desalination

Redox flow desalination batteries operate without insertion electrodes but instead uses storage into a solution phase via aqueous reactants, which decouples the capacity from the rate. This also improves round trip efficiency, the ratio of energy released from discharge over the energy input from charging and increases capacity for desalination of higher salinity influents[30]. During operation, a Zn anode is oxidized

to Zn^{2+}, driving Cl^- into the analyte tank; at the cathode, ferricyanide is reduced to ferrocyanide, driving Na^+ into the catholyte tank (Fig. 6d). This design requires an energy consumption of 2.11 kWh m^{-3} for 85% desalination of 35 part per thousand (ppt) NaCl (seawater). When combining secondary brackish water reverse osmosis with this design, hypersaline brines (100 ppt salinity) can be made potable with an energy consumption of 14.06 kWh m^{-3} as shown in Fig. 7b. Subsequent research provided a list of potential solution phase reactants for desalination[150] and improved cell architecture with the additional of a cation exchange electrode and second anion exchange membrane[151]. The cell architecture demonstrated the desalination of 203.8 ppt NaCl to 0.192 ppt over a seven stage system at an energy consumption of 84.37 kWh m^{-3}, demonstrating desalination of hypersaline brines currently not practical by non-thermal methods[151].

3.6 CDI and Faradaic Insertion Desalination Comparison

Despite significant effort and real progress in the last five decades, electrochemical deionization strategies must be further improved to supplant existing technology. While the choice of electrochemical deionization technology for a given application certainly depends on performance, it is noteworthy that "performance" is quantified by a variety of metrics, typically decided by the authors, such as ion removal rate, ion removal capacity, energy efficiency and selectivity, to name a few. Therefore, in an effort to compare deionization performance across faradaic and non-faradaic deionization mechanisms as well as feed concentration, herein we report data from several prominent references in the form of "capacity (mg g^{-1}) vs rate (mg g^{-1} min^{-1}) (Fig. 8a and b). It is important to note that non-faradaic deionization mechanisms display a roughly linear correlation between capacity and feed concentration (Fig. 8c) while faradaic mechanisms do not present with such a relationship (Fig. S1).
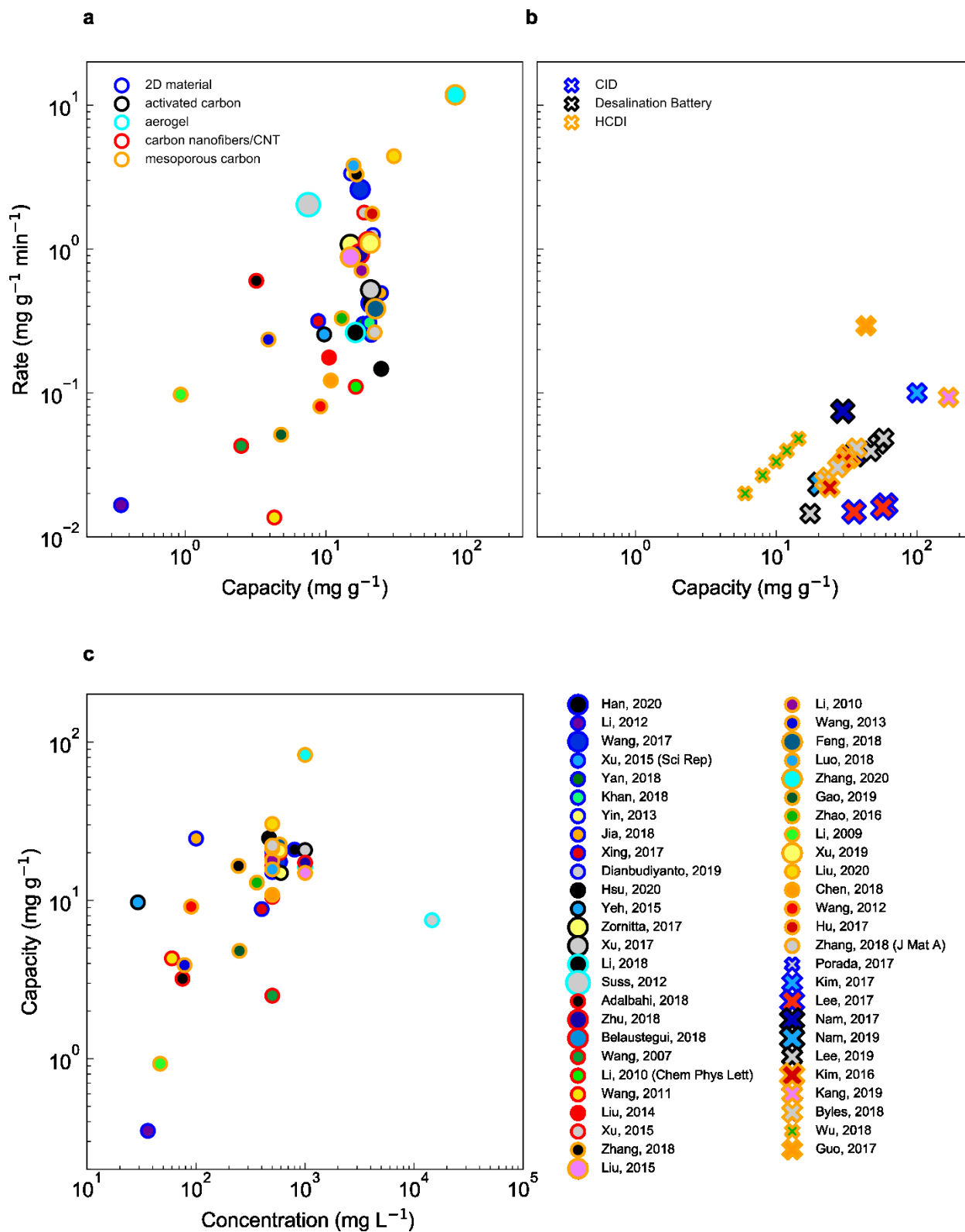
Fig. 8: Rate vs. capacity plots for CDI (a) and Faradaic insertion (b) technologies. Here, the material class is indicated by the dot outline, the reference by the unique combination of the outline and the fill color. The concentration is divided up into three categories: tap water (smallest marker size), brackish (intermediate marker size) and sea water (largest marker size). Experimental parameters, performance and references are listed in Tables S1 and S2. Average rate is calculated by dividing 95% of the electrode capacity by the time it takes to charge the electrode to the same point. CDI systems show consistently higher salt adsorption rates, relative to Faradaic insertion systems; the latter demonstrates higher capacities, however. In (c), the strong dependence of capacity on feed concentration is shown (a dependence which is not as apparent for Faradaic insertion, shown in Fig. S1).

4. Depletion Zone Desalination

A new procedure for desalination of water eschews adsorbing electrodes; instead it relies on depletion zones formed by the complex and dynamic interplay of applied electric fields, ionic diffusion and bulk water flow. Two designs of this new method, coined shock electrodialysis, have been studied to-date: one design employs an ion selective membrane or channel and the other relies purely on reaction chemistry at the electrodes.
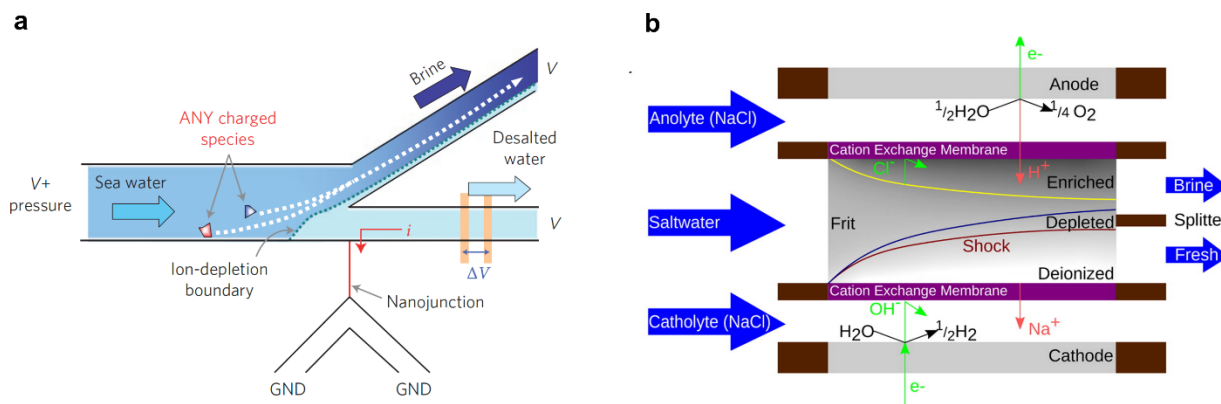
Fig. 9: (a) Nanoscale SED design where the depletion region is formed at the junction of a nanochannel and microchannel[152]. Reproduced with permission from ref. 152. Copyright 2010 Springer Nature. (b) SED device design for continuous desalination of macroscopic volumes of water between two IEMs[153]. Reproduced with permission from ref. 153. Copyright 2015 American Chemical Society.

4.1 Shock electrodialysis

Shock electrodialysis (SED) is not limited by the flow-through membranes of electrodialysis or the finite adsorption capacity of CDI. A novel method to separate ions from saline water, SED is a fundamentally nonlinear and electrokinetic phenomenon characterized by a sharp depletion region at the surface of an IEM or charge-selective nanochannel[31,154–159]. In macro-scale systems, a saline feed solution flows between two electrodes, at least one of which is coated with an IEM (usually selective for cations). By applying a voltage between these electrodes, cations flow through the IEM towards the cathode and anions are repulsed from the surface of the IEM. To retain charge neutrality at the IEM surface, a depletion region forms and at "over-limiting" currents—corresponding to faster-than-diffusion-limited ionic current—rapidly propagates outward. By placing a splitter at the boundary of the depletion region, the de-ionized water in the depletion region is permanently separated from the concentrated saline solution, effectively creating brine and deionized streams.

The phenomenon of ion-depletion near an ionically selective element was first discovered in nanofluidic structures at the interface of a microchannel and a glass nanonchannel,[160,161] and was employed as a proof-

of-concept desalination system in a single lithographically patterned device, shown in Fig. 9a [152]. This proof-of-concept displayed 99% rejection of salt in seawater with 50% of total volume conserved—i.e. the brine concentration was a factor two more concentrated than the incoming feed solution. Although this study serves as an excellent proof-of-concept, the device desalinated only tens of μL of solution and the energy efficiency of the system not optimized.

Subsequent studies turned towards larger systems with macroscopic electrodes and ion exchange membranes separated by glass frits, as shown in Fig. 9b. The negative charge on the glass frits enables the transport of ions faster than diffusion-limited speeds, without pushing the electrode voltage bias beyond 1.5 V[162]. The first of such systems effectively separated positive and negative ionic species but was not used as a desalination device. Following this initial demonstration, the same group developed a SED device that could continuously deionize a brackish feed stream[153], schematized in Fig. 9b, with a salt rejection approaching 100% and a maximum water recovery rate of 79%. The energy efficiency of this device, however, was quite poor at 10^{-1} to 10^3 kWh m^{-3}, or 0.3 to 0.003% of the thermodynamic limit. By scaling arguments, increasing the size of the device could lower energy requirement and improve efficiency[163]. While this type of device may not be applicable to large-scale desalination, it has the potential to provide small-scale desalination for various applications, which is an underdeveloped area.

A similar prototype device was shown to selectively remove (divalent) magnesium cations above (monovalent) sodium[164]. This selectivity was loosely attributed to the enhanced interaction between the divalent magnesium ions to the glass frit, slowing diffusion in the brine solution but enhancing diffusion in the depletion zone due to the surface charge mediated transport in that region. In a 9:1 $NaCl:MgCl_2$ mixture, a continuous removal of 99.06% Mg^{2+} was demonstrated, corresponding to 41.3 fold removal of Mg^{2+} over Na^+. The energy requirements remained quite high relative to reverse osmosis systems; however, these results have motivated work on the separation of multivalent ions along monovalent ions from waste streams. For the removal of radionuclides from nuclear waste streams, a three stage SED process could remove 96.3% Ce^+ and 99.6% Co^{2+} with Co^{2+} being primarily removed in the third stage[165]. Parameter

tuning allows for the optimization of Co removal, total cation removal, or water recovery ratio from a waste stream containing lithium, cobalt, and cesium. Additional water purification techniques would still be necessary to remove uncharged species such as boric acid.

4.2 Faradaic Depletion Zone Desalination

Rather than employing an ion exchange membrane or channel, one can utilize the faradaic reactions at the surface of an electrode to form an ion depletion zone (IDZ). In the first experiment of its kind, the desalination device comprised a bipolar electrode (pyrolyzed photoresist carbon) placed at the junction of a branched microchannel [166,167]. One end of the bipolar electrode acts as the cathode for water reduction and the other end as the anode for chloride oxidation (at an applied potential of 3.0 V). The chloride oxidation neutralizes the Cl^-, creating an IDZ and a local electric field gradient at the branched junction. While pressure driven flow dominates the ionic transport, ions that approach the local electric field will experience an increase in their electrophoretic velocity that drives them to the brine stream at the junction. The process was confirmed with conductivity measurements and monitoring of fluorescent dyes. This process allows for membrane-free rejection of $25\pm5\%$ salt rejection in seawater for 50% water recovery at an energy consumption of 25 Wh m^{-3} thus approaching the theoretical minimum of 17 Wh m^{-3} [168,169]. Numerical simulations have also corroborated the mechanism by coupling the mass-charge transport with the surface and volume reactions in a 3D system[170].

However, a recent study has revealed the instability of Cl_2 leads to rapid hydrolysis that quenches the IDZ. The lack of IDZ prevents its use for seawater desalination and highlights the effects electrochemical and chemical processes can have on IDZ and electric field gradients[171]. The process of forming an IDZ via Faradic reaction can still be utilized in other separations where a more stable product can be formed. Recently, the neutralization of the $TrisH^+$ buffer to the stable TrisH species to form IDZ was tested[172]. This setup demonstrated that microplastics with different electrophoretic mobilities can be sorted by using a multi-channel design at the IDZ. This platform offers many opportunities to develop membrane-free separations of charged species beyond desalination.

5. Selective Electrosorption

The systems discussed in previous Sections (excluding that of selective CDI) have applications related to complete deionization of water, e.g. desalination with the goal of making potable water from seawater and brackish sources. There is, however, a rising demand for selective electrosorption processes in which a subset of ions is adsorbed preferentially over other competitive ionic species, often present at much higher concentrations, in the same solution. These selective separations include targeted resource mining, such as uranium extraction from seawater where the relevant species, UO_2^{2+}, is present at only 3 ppb[173], and toxic water remediation. In selective electrosorption/electrodeposition, electron transfer at the electrode-electrolyte interface is coupled with a number of slower processes such as mass transport of ions into the electrical double layer (EDL), adsorption of ions and formation of an expanding ion depletion zone around the electrode before ions can be replenished near the surface. Hence, in order to achieve high capacity, fast kinetics and perhaps most importantly, high selectivity in ion extraction processes, it is important to enhance mass transport into and out of the EDL, promote specific electrode-ion interactions and mitigate depletion zone formation around the adsorbent.

Towards this common goal of efficient and selective ion extraction, researchers have developed electric field modulation techniques such as the half-wave rectified alternating current electrochemical method (HW-ACE) [34] to mitigate diffusion-limited mass transport and ion depletion zone formation. Alternating current methods are able to achieve high degrees of selectivity by exploiting a plethora of physical properties such as ionic mass, charge, radius and mobility; however, it is important to note in addition to alternating current mediated selectivity, chemical functionalization of electrodes impart selectivity to electrosorption/electrodeposition processes in different and equally important ways. For example, polymer-based electrode coatings have received a great deal of attention in recent years owing to their ability to facilitate highly specific ion interactions inside the EDL. Hence, researchers have combined the merits of alternating current methods with synthetic chemical modifications of electrodes such as the addition of chelating polymers, redox-active polymers, electroactive polymers and charged surfactants alike.

Chemical electrode coatings are typically easily synthesized, solution processible, electronically tunable and, perhaps most importantly, have molecular selectivity enabled mostly by non-covalent interactions such as electrostatic forces, Van Der Waals forces, hydrophobic effects, hydrogen bonding and π interactions. Different classes of polymers such as electroactive polymers, chelating polymers and redox-active polymers inhabit crucial roles in emerging selective electrochemical ion adsorption technologies such as the HW-ACE. This Section focuses on selective electrosorption mediated by alternating current methods, which take care of mass transport and depletion zone limitations, as well as the vast array of chemical functionalities, which facilitate highly specific ion adsorption inside the electrical double layer. While the aforementioned modes of selectivity will be addressed separately in this Section, it is important to note that the merits of alternating current techniques (Section 5.1) and chemical functionalization (Section 5.2) are often coupled to enable the high capacity, kinetically fast and highly selective electrosorption/electrodeposition behavior highlighted below.

5.1 Alternating Current Mediated Selectivity

Physicochemical adsorption methods share three intrinsic limitations: slow diffusion of ions present at low concentrations, coulombic repulsion of incoming ions by adsorbed ions of like charge and saturation of sorbent surface active sites by competing ions present at much higher concentrations than those of interest. Alternating current methods solve the conventional drawbacks of physicochemical adsorption and achieve high performance selective ion extraction. The voltage bias increases the ion collision rate in the double layer and leads to electrodeposition (neutralization) of the charged ions. The latter mitigates Coulomb repulsion and the alternating current decreases the adsorption of unwanted species and circumvents water splitting. While the selectivity of such systems is indeed driven by the alternating nature of the applied current, chemical functionalization of the electrode surface, to be discussed in further detail in a later Section (Section 5.2), is also a significant contributor towards ion selectivity.

HW-ACE was the first example of applying an alternating current to leverage highly selective ion extraction[34]. Through clever combination of alternating current and chemically induced selectivity, Cui *et al.* used HW-ACE in tandem with a poly(amidoxime) modified carbon electrode (C-Ami) as a means of extracting uranyl ions from seawater in the form of charge neutral uranium crystals (Fig. 10). HW-ACE/C-Ami achieved unprecedented uranyl selectivity versus sodium ions, nine-fold higher adsorption capacity (1932 mg g^{-1}) without saturation and four-fold faster kinetics compared to conventional diffusion-limited physicochemical adsorption.
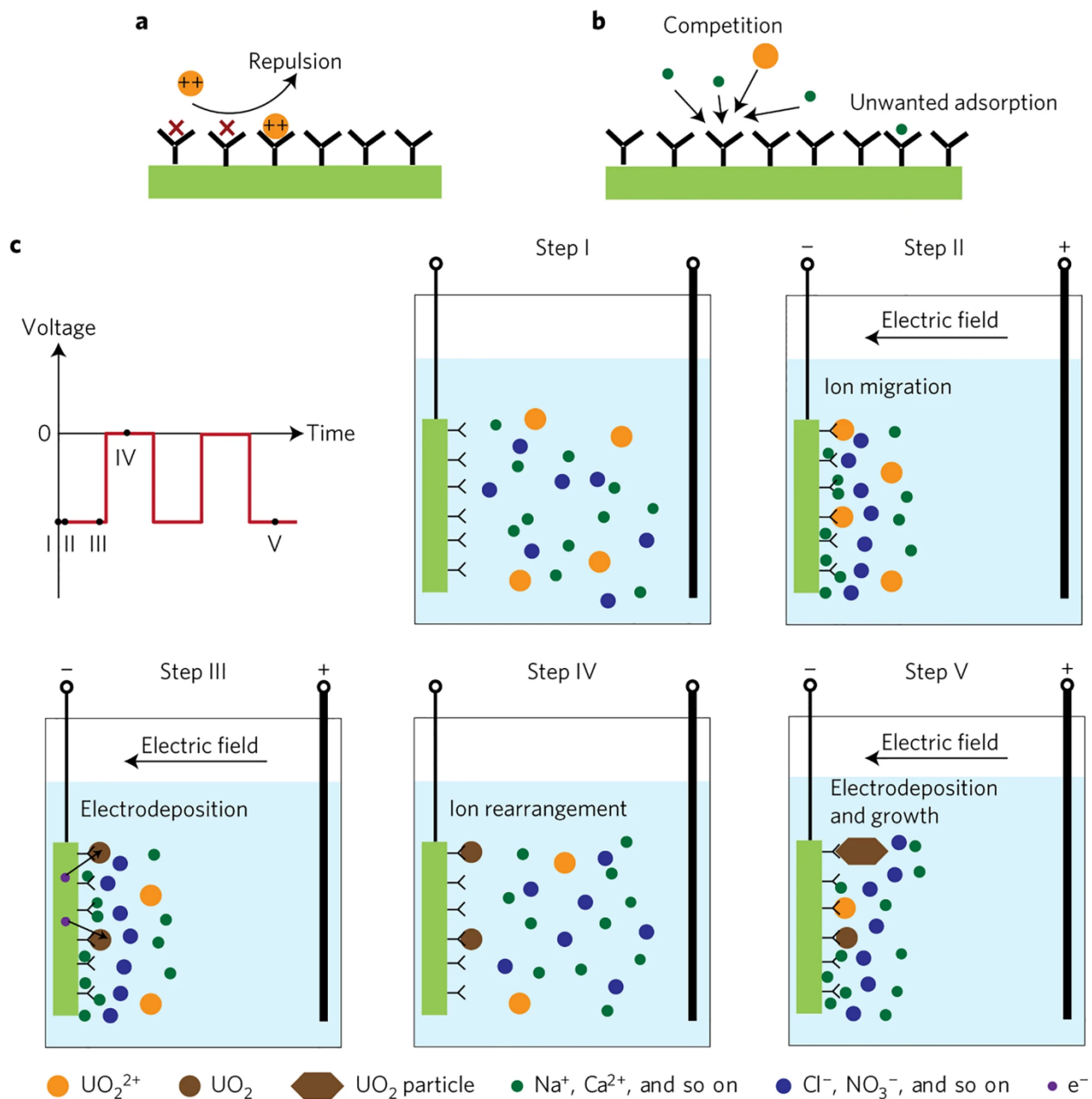
Fig. 10: Schematics of physisorption and HW-ACE (a) Schematic of coulombic repulsion of incoming ions mediated by adsorbed ions. (b) Schematic of competition between uranyl and other ions that results in blocking of active sites. (c) Outline of the extraction steps of HW-ACE. In step 1, ions are dispersed in the bulk solution; in step 2, ions migrate, form a double layer and uranyl is adsorbed; in step 3, adsorbed ions are reduced to charge-neutral UO_2; in step 4 ions are expelled when the voltage bias is removed; in step 5,

crystals grow through repetition of steps 3-5[34]. Reproduced with permission from ref. 34. Copyright 2017 Springer Nature.

In an effort to extend the success of HW-ACE/C-Ami, Cui *et al.* developed a graphene-oxide-modified carbon felt electrode (C-rGO) based electrodeposition method that can treat both low-concentration and high-concentration heavy-metal pollution using a direct/alternating current (DC/AC)[174]. DC electrodeposition with a CF-rGO electrode (DC/C-rGO) can reduce low concentrations (~300 ppb) of toxic ion mixtures (Cu, Cd, Pb) to ion concentrations within the safe drinking water range, as defined by the U.S. Environmental Protection Agency. Moreover, AC electrodeposition with a CF-rGO electrode (AC/C-rGO) can capture all three ions with capacities exceeding 29 g g^{-1} without saturation. More interestingly, AC/C-rGO can also be used to selectively extract Cu, Cd and Pb in series by leveraging the inherent differences in electrochemical reduction potential. Through the tuning of the applied electrodeposition/desorption voltages and the AC frequency, Pb, Cu and Cd (~1000 ppm each) can be sequentially extracted, in that order, to concentrations of ~1 ppm. This AC electrochemical method has also been demonstrated for successful removal of heavy metal ions from elution solutions used in soil decontamination[175].

During the performance evaluation of this device, three synthetically contaminated soil samples were prepared with 10,000 ppm Cu, 1000 ppm Pb, and 100 ppm Cd, respectively (based on typical concentrations found in contamination sites) and the asymmetrical alternating current electrochemistry (AACE) method successfully reduced the metal concentrations to below their respective California Human Health Screening Levels (CHHSL). It is important to note that the current state-of-the-art electrochemical soil remediation method applies a DC electric field to the soil to transport heavy metal species by electroosmosis and electrodeposits them to metallic states on the negative electrode. However, field application of this technology is limited by the high DC voltage required to maintain a strong electric field (~100 V m^{-1}) for electroosmosis, the low ion migration speed in soil and the large energy losses associated with water splitting at electrodes. More importantly, if a DC voltage were applied, the negative charge of the ligand complexed ionic species, metal ion-ethylenediaminetetraacetic acid (MEDTA^{2-}) would repel the negative

working electrode due to Coulombic repulsion. This example especially highlights the benefits of leveraging AC, as opposed to DC methods, in tandem with chemical electrode functionalization (C-Ami) towards highly selective electrodeposition from contaminated soil.

5.2 Chemical Functionalization

Chelating Polymers

In the previous Section, chemical functionalities were used in tandem with alternating current methods. There are, however, many examples of chelating polymers used in high performing DC electrochemical adsorption cells. The selective capability of chelating polymers—the first class of polymer coatings leveraged for selectivity in electrosorption processes—is attributed to the functional group's ability to coordinate to the metal ion. This ability is a function of several factors such as donor atom (N, O, S); ligand type (unidentate, bidentate, multidentate); ligand class (soft, intermediate or hard); and the metal-ligand complex stability constants[176–179].

In a prominent example wherein only chelating polymer electrode coatings were responsible for selective ion electrodeposition, polyamidoxime modified carbon felt (PACCF) electrodes, were used for selective electrosorption of heavy metal pollutants (Pb^{2+}, Cd^{2+}, Cu^{2+} mixture, 1000 ppm each) from point-of-use water and industrial wastewater[180]. In addition to providing for strong chelation sites, the amidoxime functionalization also helped modify the inherently hydrophobic carbon surface to hydrophilic, thus allowing for complete utilization of the carbon felt's extensive surface area. In this study, a direct current was applied to a PACCF working electrode that purified heavy metal ion contaminated water to concentrations below 5 ppb with high rates of 3000 L h^{-1} m^{-2} and displayed high capacities of 2300 mg g^{-1}.

Redox-Active Polymers

Redox-active polymers are the second major class of polymers that have been leveraged for selectivity in electrosorption processes. Since the early 1990s, many studies on redox-active polymers for

electrochemical adsorption have been published[181–185]. These sub-classes of redox-active polymers, to be discussed in detail below, undergo reversible redox reactions upon application of an electric field, which makes them especially appropriate for *selective* electrochemical separations and subsequent regeneration. Redox active polymers can generally be categorized into group-embedded polymers that possess electrochemically active backbones and pendant-bearing polymers that contain redox-active groups in their non-conductive backbone[186]. In both cases, electron transfer from the current collector to the redox-active moiety, either polymer backbone or sidechain, enables selectivity towards ionic species of interest (Fig. 11). The main example of group-embedded polymers featured in electrosorption is that of conducting polymers such as polypyrrole (PPy), polyaniline (PANi), poly(3,4-ethylenedioxythiophene):poly(4-styrenesulfonate) (PEDOT:PSS) and polyacetylene (PA). The main example of pendant bearing polymers for electrosorption is that of metallocene containing polymers also known as metallopolymers such as poly-4-vinylpyridine-metal complexes and polyvinylferrocene[187]. Indeed, group-embedded and pendant bearing structures have been combined to create metallocene containing conjugated polymers[188]. More details on applications of redox-active polymers in other fields such as energy storage are available in existing reviews[186,189,190].

Conducting Polymers

Conducting polymers—a type of group-embedded redox-active polymer—can be reversibly doped with a high degree of tunability using electrochemical methods[192–194]. Dopant ions are transported into and out of
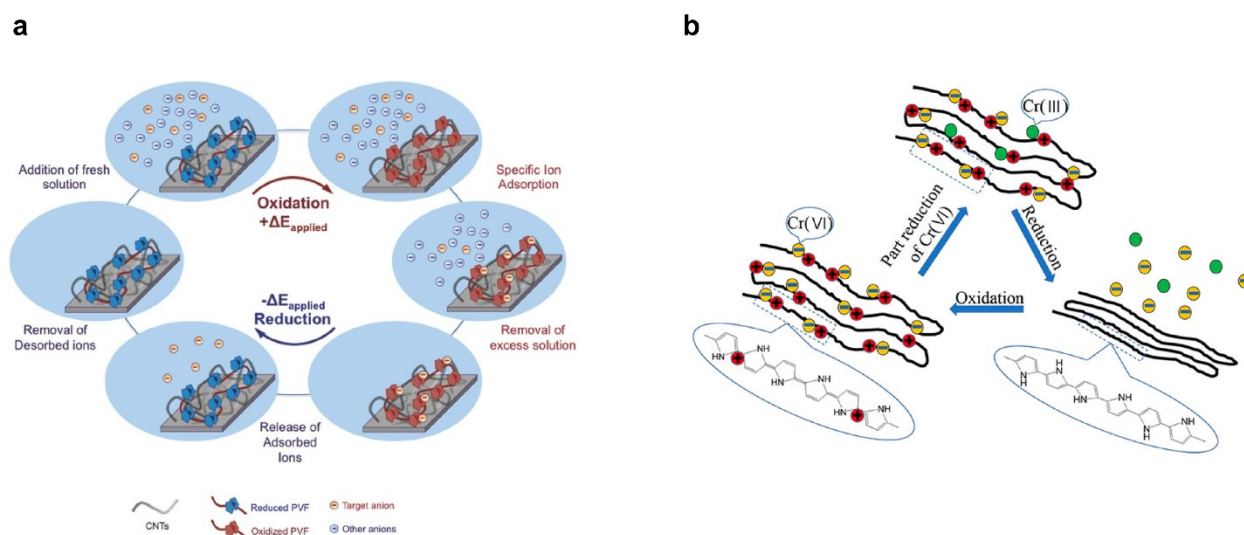
a

b

Fig. 11: (a) Redox species (PVF) mediated electrosorption and stripping of specific anions by reversible oxidation and reduction respectively[185]. Reproduced with permission from ref. 185. Copyright 2016 John Wiley and Sons. (b) Reversible electrosorption of redox-active conducting polymer polypyrrole (PPy)[191]. Reproduced with permission from ref. 191. Copyright 2018 American Chemical Society.

PPy is among the first conducting polymer to feature as an ion selective electrode coating, where the ionic permeability was switched by controlling the electronic state of the PPy backbone; the ionic permeability of chloride anions into electrodes coated with doped PPy was a factor of ~1000 greater than those coated with dedoped PPy[197,198]. A tremendous amount of work on understanding and applying the principles of electrochemically switched ion exchange has been done since[199–203]. PPy coated carbon nanotubes (PPy-CNT) have been used to selectively sequester perchlorate (ClO_4^-) anions from chloride ions that were present at a larger concentration[204]. This work was extended to include selective cation exchange processes: PPy-CNT electrodes were used for chromium (Cr(IV)) removal and subsequent reduction to Cr(III) using electrochemical potential and pH modulation[191].

While PPy is historically the most studied conducting polymer, redox-active electrosorption has been extended to PANI[205–208] and PEDOT[209] in the context of uranium separations. Pt electrodes coated with PEDOT have been for selective electrodeposition of Uranium from a mixed solution of UO_2^{2+} and Ln^{3+} (Ln = La, Ce, Sm) resulting in ~94 ± 10% stripping efficiency[210] and PANI/graphene oxide composites with large adsorption capacities of ~1960 mg g^{-1} have been used to preconcentrate uranium from highly saline aqueous solutions[211].

Metallopolymers

Metallopolymers, a sub-class of redox-active pendant-bearing chains/networks, typically consist of main-group, d-block and in some cases, f-block elements. Metallopolymers are attractive materials for a variety of applications such as energy storage, sustainable heterogeneous catalysis, photovoltaics and molecular recognition, to name a few[212–215]. Metallopolymers were first identified as prime candidates for reversible electrochemical separations in 1985. In this first work, a cation exchange styrene sulfonate-forrocene

43

copolymer adsorbed methylviologen by combining the reversible redox-activity of ferrocene and electroactivity of sulfonate[216,217]. Subsequently, Hatton *et al*. revealed the electrochemically mediated switching capability of redox-centers of metallopolymer poly(vinylferrocene) (PVF) as an efficient way to reversibly sequester small organic molecules with certain chemical functionalities (carboxylate, sulfonate, phosphonate) over others (hexafluorophosphate, perchlorate)[185,218–220]. This separation was achieved with exceptional selectivity factors of >140 and >3000 in aqueous and organic systems respectively[185]. Moreover, recent work by Hatton *et al*. demonstrates the applicability and versatility of PVF functionalized carbon redox-active electrodes (PVF-CNT) for electrochemical separations of heavy metal ions, specifically chromium and arsenic oxyanions from water[221].

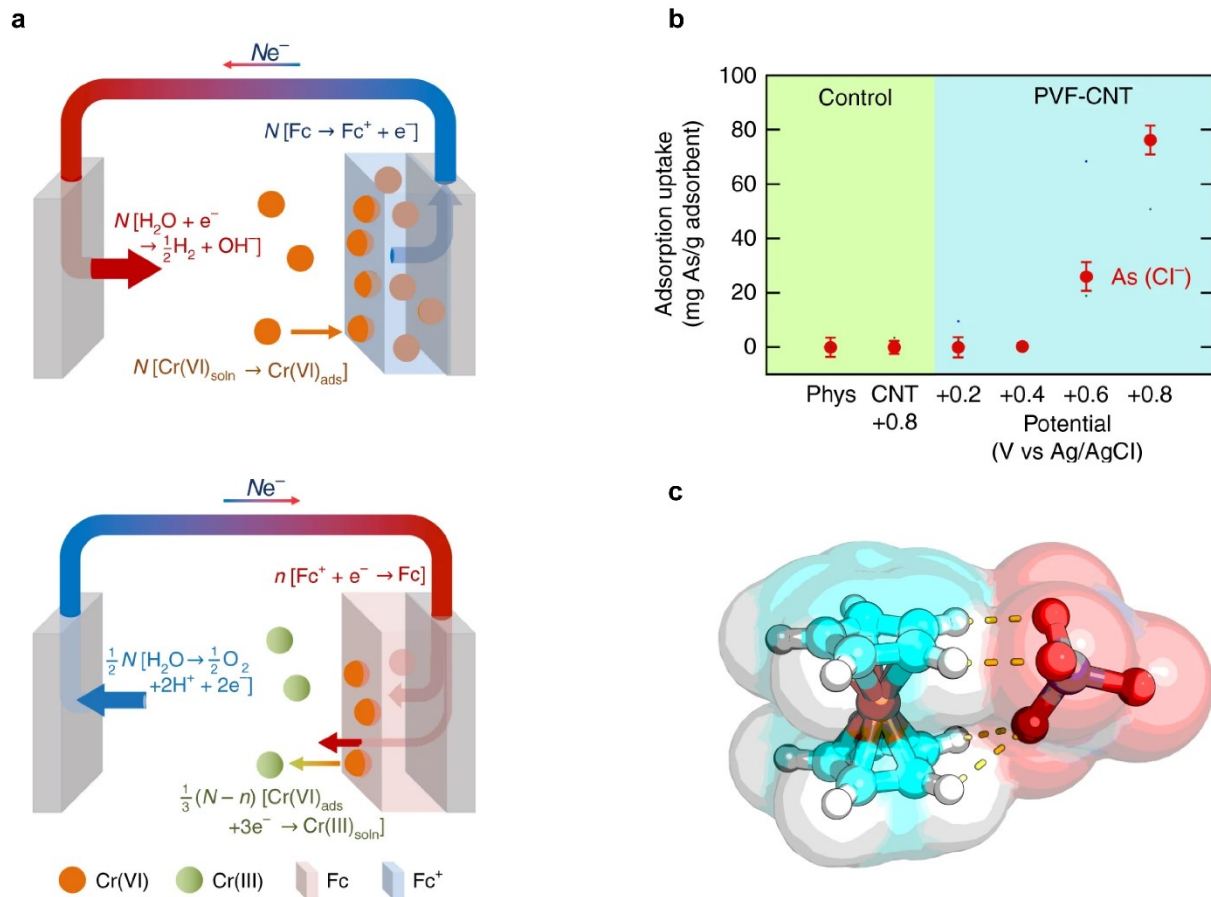Fig. 12: (a) Faradaic half-reactions occurring at electrode surface during charging/adsorption (top figure) and discharge/desorption (bottom figure)[221]. (b) Adsorption capacity of arsenate ions at 1 mM KH_2AsO_4 in

the presence of 20 mM NaCl using PVF-CNT under different applied potentials. (c) Electronic structure optimization of chromate (CrO_4^{2-}) with ferrocenium (Fc^+)[221]. Reproduced with permission from ref. 221. Copyright 2018 Springer Nature.

The PVF-CNT electrode achieved >100 mg g^{-1} capacity at saturation while retaining fast adsorption rates with 99% reversible working capacity. During adsorption, hexavalent chromium was captured at the anode surface through PVF oxidation mediated binding and during desorption, the bound chromium is reduced to the less harmful trivalent species (Fig. 12a). Remarkably higher selectivity factors and uptake capacities of chromium from water were achieved by redox-active metallopolymer electrodes relative to traditional carbon electrodes (Fig. 12b)[222]. Chromium and arsenic at 100 ppb concentrations were selectively remediated in the presence of over 200-fold excess (~2000 ppb) competing salts (NaCl). The fundamental mechanism for the selectivity of PVF towards oxyanions was elucidated via density functional theory (DFT) calculations. These calculations indicate that charge-transfer is the underlying electronic effect driving selectivity; electronic structure analysis (Fig. 12c) showed that the oxygen atoms in the chromium and arsenic anions (CrO_4^{2-}, $HAsO_4^{2-}$) are more susceptible to losing electrons to Fc^+ than are those in non-heavy metal oxyanions (ClO_4^-). Zero-temperature DFT calculations were corroborated by finite-temperature calculations that showed similar trends in selectivity with respect to heavy-metal oxyanions.

Electroactive Polymers

Another class of polymer coating for common carbon electrodes are electroactive ion-exchange polymers[223–225]. Proton-exchange polymers such as poly(2,6-pyridinedicarboxylicacid) (PDDA)[226] and poly(4-vinylpyridine)[227,228] have shown remarkable selectivity towards cupric ions among competitive monovalent and divalent ions. Researchers have shown that the selectivity of PDDA, P4VP and other proton exchange ionomers is pH switchable; selectivity can be switched on or off based on the pK_a of the exchanged proton and the pH of the electrolyte. Other examples of electroactive polymer based membranes are detailed in existing comprehensive reviews[229,230].

6. Summary and Outlook

Electrochemical ion separation is a growing field well-positioned to exploit the development of cheaper, renewable energy to fulfill the global need for potable water. In this review, we have brought together key electrochemical deionization techniques, including CDI desalination, Faradaic desalination, depletion zone desalination, and selective electrosorption. As discussed in this review, developments of these technologies have improved salt removal capacity, salt removal rate, energy consumption, and water recovery for commercial desalination. Table 2 shows the advantages and disadvantages of each desalination technology. Electrochemical ion separation methods must still overcome significant challenges to surpass existing separation technologies in industry. The long-term stability of non-Faradaic CDI must be improved by incorporating new protective materials and cell architectures to suppress side reactions and corrosion. For Faradaic CDI, protective materials must be incorporated to prevent undesired ion insertion which can initiate irreversible phase changes leading to a loss in capacity and even material failure. While we have not addressed corrosion and fouling in this review, it is a persisting issue in systems that use membranes in seawater and must be addressed when implementing a desalination technology.

Technology	Advantages	Disadvantages
Common characteristics of CDI, faradaic desalination and depletion zone desalination	• *High energy efficiency at low salt concentrations* • *All-electric operation suitable for integration with renewable energy* • *Modular and scalable*	• *Energy efficiency decreases at a faster rate than RO with increasing salt concentrations*
CDI	• Fast salt adsorption rate • High adsorption capacity (for advanced materials) • High reversibility and stability	• Capacity limited by accessible surface area
Faradaic Desalination	• High volumetric capacity • Confinement-driven ion selectivity is feasible • Low energy consumption • Redox flow design can efficiently desalinate hypersaline brines	• Slow (compared to CDI) salt adsorption rate • Most energy efficient designs use multiple layers of ion exchange membranes
Depletion Zone Desalination	• Ultrahigh (>99%) salt rejection • Robust and portable for use in small-scale desalination (i.e. crisis situations) • Not limited by finite capacity (faradaic/non-faradaic)	• Energy efficiency remains low • Difficult to deploy for large-scale desalination

	• Continuous desalination possible	
Reverse Osmosis	• Most optimized technology for brackish and seawater desalination • Low energy consumption	• Membranes susceptible to fouling and degradation • Brine disposal harmful to the environment
Electrodialysis	• High water recovery • Longer membrane lifetime than RO • Selective separation of monovalent and multivalent ions	• Membranes susceptible to fouling and degradation • High energy consumption
Thermal Distillation	• Practical method for desalination of hypersaline brines	• High energy consumption

Table 2: Comparison of desalination technologies

In forming this review, we found that a standard reporting of key metrics could improve comparison of desalination performance. The reporting of all pairs of cation removal capacity (mg of salt per g of electrode material) and average rate of ion removal (mg of salt per g of electrode per second) will facilitate easier comparison between technologies. Additionally, converting data reported as figure to both a table and figure would make easier accessibility for the reader. Regarding energy consumption, both the gravimetric specific energy (kWh per kg of salt removed) and volumetric specific energy consumptions (kWh per L of desalinate output) can help compare operation cost for technologies with the same feed concentration, water recovery, and salt removal fraction. The additional metrics to include are active material mass, total electrode mass, geometric area, flow rate, feed concentration, Coulombic efficiency, salt removal fraction, and water recovery. The use of standard conditions for brackish desalination, as proposed by Hawks et al., would also be beneficial for the field[38]. For redox flow desalination, the capacity has been fairly reported in mg of salt per liter of electrolyte solution. The comparison of this technology with others may be assisted by reporting kg of salt per g of electrolyte solution.

Beyond desalination, toxic water remediation and resource mining have been enabled by the development of selective electrosorption techniques. Ion selectivity and removal performance is enhanced for these applications via modification of standard electrodes with polymer coatings. A growing library of selective electrosorptive materials include electroactive polymers for selective CDI, chelating polymers for uranium

recovery, redox-active polymers for heavy metal ion extraction, and charged surfactants for nitrate removal. Improved understanding of ion transport and interfacial interactions will guide material selection and system design for better electrochemical deionization. This is necessary for the development of new chemistries and methods that allow for selective extraction of more dilute and uncharged species in complex solutions.

Conflicts of interest

There are no conflicts to declare

Acknowledgements

References:

1. UN DESA Population Division. World population prospects 2019: highlights. (2019).

2. Gleick, P. H. & Howe, C. W. *Water in crisis: a guide to the world's fresh water resources*. (Climatic Change, 1993).

3. Dodge, B. F. Review of distillation processes for the recovery of fresh water from saline waters. in *Saline Water Conversion—II* vol. 38 1–26 (American Chemical Society, 1963).

4. Sholl, D. S. & Lively, R. P. Seven chemical separations to change the world. *Nature* **532**, 435–437 (2016).

5. Shahzad, M. W., Burhan, M. & Ng, K. C. A standard primary energy approach for comparing desalination processes. *npj Clean Water* **2**, 1 (2019).

6. WWAP (United Nations World Water Assessment Programme). *The United Nations world water development report 2014: water and energy*. (UNESCO, 2014).

7. Elimelech, M. & Phillip, W. A. The future of seawater desalination: energy, technology, and the environment. *Science* **333**, 712–717 (2011).

8. Oren, Y. Capacitive deionization (CDI) for desalination and water treatment — past, present and future (a review). *Desalination* **228**, 10–29 (2008).

9. Porada, S., Zhao, R., van der Wal, A., Presser, V. & Biesheuvel, P. M. Review on the science and technology of water desalination by capacitive deionization. *Progress in Materials Science* **58**, 1388–1442 (2013).

10. Al-Amshawee, S. *et al.* Electrodialysis desalination for water and wastewater. *Chemical Engineering Journal* **380**, 122231 (2020).

11. Campione, A. *et al.* Electrodialysis for water desalination: A critical assessment of recent developments on process fundamentals, models and applications. *Desalination* **434**, 121–160 (2018).

12. Strathmann, H. Electrodialysis, a mature technology with a multitude of new applications. *Desalination* **264**, 268–288 (2010).

13. Biesheuvel, P. M., Fu, Y. & Bazant, M. Z. Diffuse charge and Faradaic reactions in porous electrodes. *Phys. Rev. E* **83**, 061507 (2011).

14. Biesheuvel, P. M., Porada, S., Levi, M. & Bazant, M. Z. Attractive forces in microporous carbon electrodes for capacitive deionization. *J Solid State Electrochem* **18**, 1365–1376 (2014).

15. Biesheuvel, P. M., Hamelers, H. V. M. & Suss, M. E. Theory of water desalination by porous electrodes with immobile chemical charge. *Colloids and Interface Science Communications* **9**, 1–5 (2015).

16. Caudle, D. D. *Electrochemical demineralization of water with carbon electrodes*. (U.S. Department of the Interior, 1966).

17. Oren, Y. & Soffer, A. Electrochemical parametric pumping. *J. Electrochem. Soc.* **125**, 869–875 (1978).

18. Farmer, J. C., Fix, D. V., Mack, G. V., Pekala, R. W. & Poco, J. F. Capacitive deionization of NH_4ClO_4 solutions with carbon aerogel electrodes. *J Appl Electrochem* **26**, 1007–1018 (1996).

19. Jeon, S. *et al.* Desalination via a new membrane capacitive deionization process utilizing flow-electrodes. *Energy Environ. Sci.* **6**, 1471 (2013).

20. Kim, J.-S. & Choi, J.-H. Fabrication and characterization of a carbon electrode coated with cation-exchange polymer for the membrane capacitive deionization applications. *Journal of Membrane Science* **355**, 85–90 (2010).

21. Lee, J.-B., Park, K.-K., Eum, H.-M. & Lee, C.-W. Desalination of a thermal power plant wastewater by membrane capacitive deionization. *Desalination* **196**, 125–134 (2006).

22. Avraham, E., Yaniv, B., Soffer, A. & Aurbach, D. Developing ion electroadsorption stereoselectivity, by pore size adjustment with chemical vapor deposition onto active carbon fiber electrodes. Case of Ca^{2+}/Na^+ separation in water capacitive desalination. *J. Phys. Chem. C* **112**, 7385–7389 (2008).

23. Hawks, S. A. *et al.* Using ultramicroporous carbon for the selective removal of nitrate with capacitive deionization. *Environ. Sci. Technol.* **53**, 10863–10870 (2019).

24. Kim, Y.-J., Kim, J.-H. & Choi, J.-H. Selective removal of nitrate ions by controlling the applied current in membrane capacitive deionization (MCDI). *Journal of Membrane Science* **429**, 52–57 (2013).

25. Yeo, J.-H. & Choi, J.-H. Enhancement of nitrate removal from a solution of mixed nitrate, chloride and sulfate ions using a nitrate-selective carbon electrode. *Desalination* **320**, 10–16 (2013).

26. Lado, J. J. *et al.* Removal of nitrate by asymmetric capacitive deionization. *Separation and Purification Technology* **183**, 145–152 (2017).

27. Lee, J., Kim, S., Kim, C. & Yoon, J. Hybrid capacitive deionization to enhance the desalination performance of capacitive techniques. *Energy Environ. Sci.* **7**, 3683–3689 (2014).

28. Pasta, M., Wessells, C. D., Cui, Y. & La Mantia, F. A desalination battery. *Nano Lett.* **12**, 839–843 (2012).

29. Smith, K. C. & Dmello, R. Na-ion desalination (NID) enabled by Na-blocking membranes and symmetric Na-intercalation: porous-electrode modeling. *J. Electrochem. Soc.* **163**, A530–A539 (2016).

30. Desai, D. *et al.* Electrochemical desalination of seawater and hypersaline brines with coupled electricity storage. *ACS Energy Lett.* **3**, 375–379 (2018).

31. Mani, A. & Bazant, M. Z. Deionization shocks in microstructures. *Phys. Rev. E* **84**, 061504 (2011).

32. Oyarzun, D. I., Hemmatifar, A., Palko, J. W., Stadermann, M. & Santiago, J. G. Ion selectivity in capacitive deionization with functionalized electrode: theory and experimental validation. *Water Research X* **1**, 100008 (2018).

33. Oyarzun, D. I., Hemmatifar, A., Palko, J. W., Stadermann, M. & Santiago, J. G. Adsorption and capacitive regeneration of nitrate using inverted capacitive deionization with surfactant functionalized carbon electrodes. *Separation and Purification Technology* **194**, 410–415 (2018).

34. Liu, C. *et al.* A half-wave rectified alternating current electrochemical method for uranium extraction from seawater. *Nat Energy* **2**, 17007 (2017).

35. Su, X. *et al.* Electrochemically-mediated selective capture of heavy metal chromium and arsenic oxyanions from water. *Nat Commun* **9**, 4701 (2018).

36. Suss, M. E. *et al.* Water desalination via capacitive deionization: what is it and what can we expect from it? *Energy Environ. Sci.* **8**, 2296–2319 (2015).

37. Kim, T. & Yoon, J. CDI ragone plot as a functional tool to evaluate desalination performance in capacitive deionization. *RSC Adv.* **5**, 1456–1461 (2014).

38. Hawks, S. A. *et al.* Performance metrics for the objective assessment of capacitive deionization systems. *Water Research* **152**, 126–137 (2019).

39. Wang, H. *et al.* Three-dimensional macroporous graphene architectures as high performance electrodes for capacitive deionization. *Journal of Materials Chemistry A* **1**, 11778–11789 (2013).

40. Zhao, R., M. Biesheuvel, P. & Wal, A. van der. Energy consumption and constant current operation in membrane capacitive deionization. *Energy & Environmental Science* **5**, 9520–9527 (2012).

41. Wang, L., Dykstra, J. E. & Lin, S. Energy efficiency of capacitive deionization. *Environ. Sci. Technol.* **53**, 3366–3378 (2019).

42. Wang, L. & Lin, S. Intrinsic tradeoff between kinetic and energetic efficiencies in membrane capacitive deionization. *Water Research* **129**, 394–401 (2018).

43. Hand, S., Shang, X., Guest, J. S., Smith, K. C. & Cusick, R. D. Global sensitivity analysis to characterize operational limits and prioritize performance goals of capacitive deionization technologies. *Environ. Sci. Technol.* **53**, 3748–3756 (2019).

44. Liu, T. *et al.* Exceptional capacitive deionization rate and capacity by block copolymer–based porous carbon fibers. *Science Advances* **6**, eaaz0906 (2020).

45. Oladunni, J. *et al.* A comprehensive review on recently developed carbon based nanocomposites for capacitive deionization: From theory to practice. *Separation and Purification Technology* **207**, 291–320 (2018).

46. Jia, B. & Zhang, W. Preparation and application of electrodes in capacitive deionization (CDI): a state-of-art review. *Nanoscale Research Letters* **11**, 64 (2016).

47. Yeh, C.-L., Hsi, H.-C., Li, K.-C. & Hou, C.-H. Improved performance in capacitive deionization of activated carbon electrodes with a tunable mesopore and micropore ratio. *Desalination* **367**, 60–68 (2015).

48. Kim, Y.-J. & Choi, J.-H. Enhanced desalination efficiency in capacitive deionization with an ion-selective membrane. *Separation and Purification Technology* **71**, 70–75 (2010).

49. Nadakatti, S., Tendulkar, M. & Kadam, M. Use of mesoporous conductive carbon black to enhance performance of activated carbon electrodes in capacitive deionization technology. *Desalination* **268**, 182–188 (2011).

50. Chen, Z. *et al.* A study of the effect of carbon characteristics on capacitive deionization (CDI) performance. *Desalination* **433**, 68–74 (2018).

51. Li, H., Pan, L., Nie, C., Liu, Y. & Sun, Z. Reduced graphene oxide and activated carbon composites for capacitive deionization. *J. Mater. Chem.* **22**, 15556–15561 (2012).

52. Zornitta, R. L. *et al.* High-performance activated carbon from polyaniline for capacitive deionization. *Carbon* **123**, 318–333 (2017).

53. Hsu, C.-C., Tu, Y.-H., Yang, Y.-H., Wang, J.-A. & Hu, C.-C. Improved performance and long-term stability of activated carbon doped with nitrogen for capacitive deionization. *Desalination* **481**, 114362 (2020).

54. Pekala, R. W. *et al.* Carbon aerogels for electrochemical applications. *Journal of Non-Crystalline Solids* **225**, 74–80 (1998).

55. Li, L., Zou, L., Song, H. & Morris, G. Ordered mesoporous carbons synthesized by a modified sol–gel process for electrosorptive removal of sodium chloride. *Carbon* **47**, 775–781 (2009).

56. Liu, Y. *et al.* Carbon aerogels electrode with reduced graphene oxide additive for capacitive deionization with enhanced performance. *Inorganic Chemistry Frontiers* **1**, 249–255 (2014).

57. Luo, G., Wang, Y., Gao, L., Zhang, D. & Lin, T. Graphene bonded carbon nanofiber aerogels with high capacitive deionization capability. *Electrochimica Acta* **260**, 656–663 (2018).

58. Liu, X. *et al.* Nitrogen-doped hierarchical porous carbon aerogel for high-performance capacitive deionization. *Separation and Purification Technology* **224**, 44–50 (2019).

59. Li, H., Lu, T., Pan, L., Zhang, Y. & Sun, Z. Electrosorption behavior of graphene in NaCl solutions. *J. Mater. Chem.* **19**, 6773–6779 (2009).

60. Li, H., Zou, L., Pan, L. & Sun, Z. Novel graphene-like electrodes for capacitive deionization. *Environ. Sci. Technol.* **44**, 8692–8697 (2010).

61. Yang, Z.-Y. *et al.* Sponge-templated preparation of high surface area graphene with ultrahigh capacitive deionization performance. *Advanced Functional Materials* **24**, 3917–3925 (2014).

62. Dianbudiyanto, W. & Liu, S.-H. Outstanding performance of capacitive deionization by a hierarchically porous 3D architectural graphene. *Desalination* **468**, 114069 (2019).

63. Han, D.-C. *et al.* High-performance capacitive deionization using nitrogen and phosphorus-doped three-dimensional graphene with tunable pore size. *Electrochimica Acta* **336**, 135639 (2020).

64. Wimalasiri, Y. & Zou, L. Carbon nanotube/graphene composite for enhanced capacitive deionization performance. *Carbon* **59**, 464–471 (2013).

65. Amiri, A., Chen, Y., Bee Teng, C. & Naraghi, M. Porous nitrogen-doped MXene-based electrodes for capacitive deionization. *Energy Storage Materials* **25**, 731–739 (2020).

66. Chen, B. *et al.* MXene as a Cation-Selective Cathode Material for Asymmetric Capacitive Deionization. *ACS Appl. Mater. Interfaces* **12**, 13750–13758 (2020).

67. Peng, W., Wang, W., Han, G., Huang, Y. & Zhang, Y. Fabrication of 3D flower-like MoS2/graphene composite as high-performance electrode for capacitive deionization. *Desalination* **473**, 114191 (2020).

68. Xing, F. *et al.* Chemically exfoliated MoS_2 for capacitive deionization of saline water. *Nano Energy* **31**, 590–595 (2017).

69. Gao, T. *et al.* Mesoporous carbon derived from ZIF-8 for high efficient electrosorption. *Desalination* **451**, 133–138 (2019).

70. Zhao, S. *et al.* High capacity and high rate capability of nitrogen-doped porous hollow carbon spheres for capacitive deionization. *Applied Surface Science* **369**, 460–469 (2016).

71. Tsouris, C. *et al.* Mesoporous Carbon for Capacitive Deionization of Saline Water. *Environ. Sci. Technol.* **45**, 10243–10249 (2011).

72. Xu, X. *et al.* Capacitive deionization using nitrogen-doped mesostructured carbons for highly efficient brackish water desalination. *Chemical Engineering Journal* **362**, 887–896 (2019).

73. Zhang, P., Li, J. & Chan-Park, M. B. Hierarchical Porous Carbon for High-Performance Capacitive Desalination of Brackish Water. *ACS Sustainable Chem. Eng.* **8**, 9291–9300 (2020).

74. Lee, J.-B., Park, K.-K., Eum, H.-M. & Lee, C.-W. Desalination of a thermal power plant wastewater by membrane capacitive deionization. *Desalination* **196**, 125–134 (2006).

75. Hassanvand, A., Wei, K., Talebi, S., Chen, G. Q. & Kentish, S. E. The role of ion exchange membranes in membrane capacitive deionisation. *Membranes* **7**, 54 (2017).

76. Kim, Y.-J. & Choi, J.-H. Improvement of desalination efficiency in capacitive deionization using a carbon electrode coated with an ion-exchange polymer. *Water Research* **44**, 990–996 (2010).

77. Wang, L. & Lin, S. Mechanism of selective ion removal in membrane capacitive deionization for water softening. *Environ. Sci. Technol.* **53**, 5797–5804 (2019).

78. Ma, J. *et al.* Carbon black flow electrode enhanced electrochemical desalination using single-cycle operation. *Environ. Sci. Technol.* **54**, 1177–1185 (2020).

79. Oren, Y. Capacitive deionization (CDI) for desalination and water treatment — past, present and future (a review). *Desalination* **228**, 10–29 (2008).

80. Suss, M. E. *et al.* Capacitive desalination with flow-through electrodes. *Energy Environ. Sci.* **5**, 9511–9519 (2012).

81. Jeon, S. *et al.* Desalination via a new membrane capacitive deionization process utilizing flow-electrodes. *Energy Environ. Sci.* **6**, 1471 (2013).

82. He, C., Ma, J., Zhang, C., Song, J. & Waite, T. D. Short-circuited closed-cycle operation of flow-electrode CDI for brackish water softening. *Environ. Sci. Technol.* **52**, 9350–9360 (2018).

83. Ma, J. *et al.* Water recovery rate in short-circuited closed-cycle operation of flow-electrode capacitive deionization (FCDI). *Environ. Sci. Technol.* **53**, 13859–13867 (2019).

84. Tang, K., Yiacoumi, S., Li, Y. & Tsouris, C. Enhanced water desalination by increasing the electroconductivity of carbon powders for high-performance flow-electrode capacitive deionization. *ACS Sustainable Chem. Eng.* **7**, 1085–1094 (2019).

85. Liu, S., Do, V. Q. & Smith, K. C. Modeling of electrochemical deionization across length scales: Recent accomplishments and new opportunities. *Current Opinion in Electrochemistry* **22**, 72–79 (2020).

86. Bazant, M. Z., Thornton, K. & Ajdari, A. Diffuse-charge dynamics in electrochemical systems. *Phys. Rev. E* **70**, 021506 (2004).

87. Biesheuvel, P. M. & Bazant, M. Z. Nonlinear dynamics of capacitive charging and desalination by porous electrodes. *Phys. Rev. E* **81**, 031502 (2010).

88. Johnson, A. M. & Newman, J. Desalting by Means of Porous Carbon Electrodes. *J. Electrochem. Soc.* **118**, 510 (1971).

89. Biesheuvel, P. M., Fu, Y. & Bazant, M. Z. Diffuse charge and Faradaic reactions in porous electrodes. *Phys. Rev. E* **83**, 061507 (2011).

90. Murad, M. A. & Moyne, C. A dual-porosity model for ionic solute transport in expansive clays. *Comput Geosci* **12**, 47 (2007).

91. Revil, A. & Linde, N. Chemico-electromechanical coupling in microporous media. *Journal of Colloid and Interface Science* **302**, 682–694 (2006).

92. Hemmatifar, A., Stadermann, M. & Santiago, J. G. Two-dimensional porous electrode model for capacitive deionization. *J. Phys. Chem. C* **119**, 24681–24694 (2015).

93. Simoncelli, M. *et al.* Blue Energy and Desalination with Nanoporous Carbon Electrodes: Capacitance from Molecular Simulations to Continuous Models. *Phys. Rev. X* **8**, 021024 (2018).

94. Shocron, A. N. & Suss, M. E. The effect of surface transport on water desalination by porous electrodes undergoing capacitive charging. *J. Phys.: Condens. Matter* **29**, 084003 (2017).

95. Shang, X., Cusick, R. D. & Smith, K. C. A combined modeling and experimental study assessing the impact of fluid pulsation on charge and energy efficiency in capacitive deionization. *J. Electrochem. Soc.* **164**, E536–E547 (2017).

96. Porada, S. *et al.* Direct prediction of the desalination performance of porous carbon electrodes for capacitive deionization. *Energy Environ. Sci.* **6**, 3700 (2013).

97. Porada, S. *et al.* Water desalination using capacitive deionization with microporous carbon electrodes. *ACS Appl. Mater. Interfaces* **4**, 1194–1199 (2012).

98. Nordstrand, J. & Dutta, J. Dynamic Langmuir Model: A Simpler Approach to Modeling Capacitive Deionization. *J. Phys. Chem. C* **123**, 16479–16485 (2019).

99. Nordstrand, J. & Dutta, J. Simplified Prediction of Ion Removal in Capacitive Deionization of Multi-Ion Solutions. *Langmuir* **36**, 1338–1344 (2020).

100. Lee, D.-H. *et al.* Selective lithium recovery from aqueous solution using a modified membrane capacitive deionization system. *Hydrometallurgy* **173**, 283–288 (2017).

101. Siekierka, A. & Bryjak, M. Hybrid capacitive deionization with anion-exchange membranes for lithium extraction. *E3S Web Conf.* **22**, 00157 (2017).

102. Oyarzun, D. I., Hemmatifar, A., Palko, J. W., Stadermann, M. & Santiago, J. G. Adsorption and capacitive regeneration of nitrate using inverted capacitive deionization with surfactant functionalized carbon electrodes. *Separation and Purification Technology* **194**, 410–415 (2018).

103. Tang, W., Kovalsky, P., Cao, B., He, D. & Waite, T. D. Fluoride removal from brackish groundwaters by constant current capacitive deionization (CDI). *Environ. Sci. Technol.* **50**, 10570–10579 (2016).

104. Gabelich, C. J., Tran, T. D. & Suffet, I. H. "Mel". Electrosorption of inorganic salts from aqueous solution using carbon aerogels. *Environ. Sci. Technol.* **36**, 3010–3019 (2002).

105.   Seo, S.-J. *et al.* Investigation on removal of hardness ions by capacitive deionization (CDI) for

water softening applications. *Water Res.* **44**, 2267–2275 (2010).

106.   Conway, B. E. Transition from "supercapacitor" to "battery" behavior in electrochemical energy

storage. *J. Electrochem. Soc.* **138**, 1539 (1991).

107.   Porada, S., Shrivastava, A., Bukowska, P., Biesheuvel, P. M. & Smith, K. C. Nickel

hexacyanoferrate electrodes for continuous cation intercalation desalination of brackish water.

Electrochimica Acta **255**, 369–378 (2017).

108.   Kim, H. *et al.* Aqueous rechargeable Li and Na ion batteries. *Chem. Rev.* **114**, 11788–11827

(2014).

109.   Singh, K., Porada, S., de Gier, H. D., Biesheuvel, P. M. & de Smet, L. C. P. M. Timeline on the

application of intercalation materials in Capacitive Deionization. *Desalination* **455**, 115–134 (2019).

110.   Yoon, H., Lee, J., Kim, S. & Yoon, J. Review of concepts and applications of electrochemical ion

separation (EIONS) process. *Separation and Purification Technology* **215**, 190–207 (2019).

111.   Li, W., Dahn, J. R. & Wainwright, D. S. Rechargeable lithium batteries with aqueous electrolytes.

Science **264**, 1115–1118 (1994).

112.   Luo, J.-Y., Cui, W.-J., He, P. & Xia, Y.-Y. Raising the cycling stability of aqueous lithium-ion

batteries by eliminating oxygen in the electrolyte. *Nature Chem* **2**, 760–765 (2010).

113.   Pan, H., Hu, Y.-S. & Chen, L. Room-temperature stationary sodium-ion batteries for large-scale

electric energy storage. *Energy Environ. Sci.* **6**, 2338 (2013).

114.   Kim, H. *et al.* New iron-based mixed-polyanion cathodes for lithium and sodium rechargeable

batteries: combined first principles calculations and experimental study. *J. Am. Chem. Soc.* **134**,

10369–10372 (2012).

115.   Park, Y.-U. *et al.* A new high-energy cathode for a Na-ion battery with ultrahigh stability. *J. Am.

Chem. Soc.* **135**, 13870–13878 (2013).

116.   Sauvage, F., Baudrin, E. & Tarascon, J.-M. Study of the potentiometric response towards sodium

ions of $Na_{0.44}$–$xMnO_2$ for the development of selective sodium ion sensors. *Sensors and Actuators B:*

Chemical **120**, 638–644 (2007).

117.   Whitacre, J. F., Tevar, A. & Sharma, S. $Na_4Mn_9O_{18}$ as a positive electrode material for an aqueous

electrolyte sodium-ion energy storage device. *Electrochemistry Communications* **12**, 463–466

(2010).

118.   Lee, J., Kim, S., Kim, C. & Yoon, J. Hybrid capacitive deionization to enhance the desalination

performance of capacitive techniques. *Energy Environ. Sci.* **7**, 3683–3689 (2014).

119.   Jung, Y. H., Lim, C. H., Kim, J.-H. & Kim, D. K. $Na_2FeP_2O_7$ as a positive electrode material for

rechargeable aqueous sodium-ion batteries. *RSC Adv.* **4**, 9799 (2014).

120.   Kim, S., Lee, J., Kim, C. & Yoon, J. $Na_2FeP_2O_7$ as a novel material for hybrid capacitive

deionization. *Electrochimica Acta* **203**, 265–271 (2016).

121.   Song, W. *et al.* Aqueous sodium-ion battery using a $Na_3V_2(PO_4)_3$electrode. *CHEMELECTROCHEM*

1, 871–876 (2014).

122.   Zhao, W., Guo, L., Ding, M., Huang, Y. & Yang, H. Y. Ultrahigh-desalination-capacity dual-ion

electrochemical deionization device based on $Na_3V_2(PO_4)_3$@C–AgCl electrodes. *ACS Appl. Mater.*

Interfaces **10**, 40540–40548 (2018).

123.   Nam, D.-H. & Choi, K.-S. Bismuth as a new chloride-storage electrode enabling the construction

of a practical high capacity desalination battery. *J. Am. Chem. Soc.* **139**, 11055–11063 (2017).

124.   Park, S. I., Gocheva, I., Okada, S. & Yamaki, J. Electrochemical properties of $NaTi_2(PO_4)_3$ anode

for rechargeable aqueous sodium-ion batteries. *J. Electrochem. Soc.* **158**, A1067 (2011).

125.   Pasta, M. *et al.* Full open-framework batteries for stationary energy storage. *Nat Commun* **5**,

3007 (2014).

126.   Wang, R. Y., Wessells, C. D., Huggins, R. A. & Cui, Y. Highly reversible open framework nanoscale electrodes for divalent ion batteries. *Nano Lett.* **13**, 5748–5752 (2013).

127.   Guo, L. *et al.* A Prussian blue anode for high performance electrochemical deionization promoted by the faradaic mechanism. *Nanoscale* **9**, 13305–13312 (2017).

128.   Choi, S. *et al.* Battery electrode materials with omnivalent cation storage for fast and charge-efficient ion removal of asymmetric capacitive deionization. *Adv. Funct. Mater.* **28**, 1802665 (2018).

129.   Chen, F. *et al.* Dual-ions electrochemical deionization: a desalination generator. *Energy Environ. Sci.* **10**, 2081–2089 (2017).

130.   Kim, S. *et al.* Hybrid electrochemical desalination system combined with an oxidation process. *ACS Sustainable Chem. Eng.* **6**, 1620–1626 (2018).

131.   Srimuk, P. *et al.* Two-dimensional molybdenum carbide (MXene) with divacancy ordering for brackish and seawater desalination via cation and anion intercalation. *ACS Sustainable Chem. Eng.* **6**, 3739–3747 (2018).

132.   Srimuk, P. *et al.* MXene as a novel intercalation-type pseudocapacitive cathode and anode for capacitive deionization. *J. Mater. Chem. A* **4**, 18265–18271 (2016).

133.   Lukatskaya, M. R. *et al.* Cation intercalation and high volumetric capacitance of two-dimensional titanium carbide. *Science* **341**, 1502–1505 (2013).

134.   Anderson, S. C. Mineral Industry Surveys. (2017).

135.   Bennett, S. M. Mineral Industry Surveys. (2017).

136.   Nam, D.-H., Lumley, M. A. & Choi, K.-S. A desalination battery Combining $Cu_3[Fe(CN)_6]_2$ as a Na-storage electrode and Bi as a Cl-storage electrode enabling membrane-free desalination. *Chem. Mater.* **31**, 1460–1468 (2019).

137.   Lee, J. *et al.* Enhancement in desalination performance of battery electrodes via improved mass transport using a multichannel flow system. *ACS Appl. Mater. Interfaces* **11**, 36580–36588 (2019).

138.   Byles, B. W., Cullen, D. A., More, K. L. & Pomerantseva, E. Tunnel structured manganese oxide

        nanowires as redox active electrodes for hybrid capacitive deionization. *Nano Energy* **44**, 476–488

        (2018).

139.   Wu, T. *et al.* Highly stable hybrid capacitive deionization with a MnO_2 anode and a positively

        charged cathode. *Environ. Sci. Technol. Lett.* **5**, 98–102 (2018).

140.   Byles, B. W., Hayes-Oberst, B. & Pomerantseva, E. Ion removal performance,

        structural/compositional dynamics, and electrochemical stability of layered manganese oxide

        electrodes in hybrid capacitive deionization. *ACS Appl. Mater. Interfaces* **10**, 32313–32322 (2018).

141.   Wang, K. *et al.* Metal–organic-frameworks-derived $NaTi_2(PO_4)_3$/carbon composites for

        efficient hybrid capacitive deionization. *J. Mater. Chem. A* **7**, 12126–12133 (2019).

142.   Fuller, T. F. Simulation and optimization of the dual lithium ion insertion cell. *J. Electrochem. Soc.*

        141, 1 (1994).

143.   Smith, K. C. Theoretical evaluation of electrochemical cell architectures using cation

        intercalation electrodes for desalination. *Electrochimica Acta* **230**, 333–341 (2017).

144.   Liu, S. & Smith, K. C. Quantifying the trade-offs between energy consumption and salt removal

        rate in membrane-free cation intercalation desalination. *Electrochimica Acta* **271**, 652–665 (2018).

145.   Singh, K., Bouwmeester, H. J. M., de Smet, L. C. P. M., Bazant, M. Z. & Biesheuvel, P. M. Theory

        of water desalination with intercalation materials. *Phys. Rev. Applied* **9**, 064036 (2018).

146.   Kim, T., Gorski, C. A. & Logan, B. E. Low energy desalination using battery electrode deionization.

        Environ. Sci. Technol. Lett. **4**, 444–449 (2017).

147.   Lee, J., Kim, S. & Yoon, J. Rocking chair desalination battery based on prussian blue electrodes.

        ACS Omega **2**, 1653–1659 (2017).

148.   Wessells, C. D., Peddada, S. V., Huggins, R. A. & Cui, Y. Nickel hexacyanoferrate nanoparticle

        electrodes for aqueous sodium and potassium ion batteries. *Nano Lett.* **11**, 5421–5425 (2011).

149.   Ahn, J. *et al.* High performance electrochemical saline water desalination using silver and silver-chloride electrodes. *Desalination* **476**, 114216 (2020).

150.   Hou, X. *et al.* Coupling desalination and energy storage with redox flow electrodes. *Nanoscale* **10**, 12308–12314 (2018).

151.   Beh, E. S., Benedict, M. A., Desai, D. & Rivest, J. B. A redox-shuttled electrochemical method for energy-efficient separation of salt from water. *ACS Sustainable Chemistry & Engineering* **7**, 13411–13417 (2019).

152.   Kim, S. J., Ko, S. H., Kang, K. H. & Han, J. Direct seawater desalination by ion concentration polarization. *Nature Nanotech* **5**, 297–301 (2010).

153.   Schlumpberger, S., Lu, N. B., Suss, M. E. & Bazant, M. Z. Scalable and continuous water deionization by shock electrodialysis. *Environ. Sci. Technol. Lett.* **2**, 367–372 (2015).

154.   Kim, S. J., Wang, Y.-C., Lee, J. H., Jang, H. & Han, J. Concentration polarization and nonlinear electrokinetic flow near a nanofluidic channel. *Phys. Rev. Lett.* **99**, 044501 (2007).

155.   Mani, A., Zangle, T. A. & Santiago, J. G. On the propagation of concentration polarization from microchannel–nanochannel interfaces part I: analytical model and characteristic analysis. *Langmuir* **25**, 3898–3908 (2009).

156.   Zangle, T. A., Mani, A. & Santiago, J. G. On the propagation of concentration polarization from microchannel–nanochannel interfaces part II: numerical and experimental study. *Langmuir* **25**, 3909–3916 (2009).

157.   Dydek, E. V. *et al.* Overlimiting current in a microchannel. *Phys. Rev. Lett.* **107**, 118301 (2011).

158.   Dydek, E. V. & Bazant, M. Z. Nonlinear dynamics of ion concentration polarization in porous media: The leaky membrane model. *AIChE J.* **59**, 3539–3555 (2013).

159.   Deng, D. *et al.* Overlimiting current and shock electrodialysis in porous media. *Langmuir* **29**, 16167–16177 (2013).

160.   Pu, Q., Yun, J., Temkin, H. & Liu, S. Ion-enrichment and ion-depletion effect of nanochannel

structures. *Nano Lett.* **4**, 1099–1103 (2004).

161.   Wang, Y.-C., Stevens, A. L. & Han, J. Million-fold preconcentration of proteins and peptides by

nanofluidic filter. *Anal. Chem.* **77**, 4293–4299 (2005).

162.   Deng, D. *et al.* Water purification by shock electrodialysis: deionization, filtration, separation,

and disinfection. *Desalination* **357**, 77–83 (2015).

163.   Alkhadra, M. A., Gao, T., Conforti, K. M., Tian, H. & Bazant, M. Z. Small-scale desalination of

seawater by shock electrodialysis. *Desalination* **476**, 114219 (2020).

164.   Conforti, K. M. & Bazant, M. Z. Continuous ion-selective separations by shock electrodialysis.

AIChE J (2019) doi:10.1002/aic.16751.

165.   Alkhadra, M. A., Conforti, K. M., Gao, T., Tian, H. & Bazant, M. Z. Continuous Separation of

Radionuclides from Contaminated Water by Shock Electrodialysis. *Environ. Sci. Technol.*

acs.est.9b05380 (2019) doi:10.1021/acs.est.9b05380.

166.   Knust, K. N., Hlushkou, D., Anand, R. K., Tallarek, U. & Crooks, R. M. Electrochemically mediated

seawater desalination. *Angewandte Chemie International Edition* **52**, 8107–8110 (2013).

167.   Dhopeshwarkar, R., Hlushkou, D., Nguyen, M., Tallarek, U. & Crooks, R. M. Electrokinetics in

Microfluidic Channels Containing a Floating Electrode. *J. Am. Chem. Soc.* **130**, 10480–10481 (2008).

168.   Cerci, Y., Cengel, Y. A. & Wood, B. The minimum separation work for desalination processes.

Proc. ASME Adv. Energy Syst. Div. **39**, 545–552 (1999).

169.   Cengel, Y. A., Cerci, Y. & Wood, B. Second law analysis of separation processes of mixtures,.

Proc. ASME Adv. Energy Syst. Div. **39**, 537–543 (1999).

170.   Hlushkou, D., Knust, K. N., Crooks, R. M. & Tallarek, U. Numerical simulation of electrochemical

desalination. *J. Phys.: Condens. Matter* **28**, 194001 (2016).

171.   Davies, C. D., Johnson, S. E. & Crooks, R. M. Effect of Chloride Oxidation on Local Electric Fields

        in Microelectrochemical Systems. *ChemElectroChem* **6**, 4867–4876 (2019).

172.   Davies, C. D. & Crooks, R. M. Focusing, sorting, and separating microplastics by serial faradaic

        ion concentration polarization. *Chem. Sci.* **11**, 5547–5558 (2020).

173.   Tabushi, I., Kobuke, Y. & Nishiya, T. Extraction of uranium from seawater by polymer-bound

        macrocyclic hexaketone. *Nature* **280**, 665–666 (1979).

174.   Liu, C. *et al.* Direct/alternating current electrochemical method for removing and recovering

        heavy metal from water using graphene oxide electrode. *ACS Nano* **13**, 6431–6437 (2019).

175.   Xu, J. *et al.* Remediation of heavy metal contaminated soil by asymmetrical alternating current

        electrochemistry. *Nat Commun* **10**, 2440 (2019).

176.   Myasoedova, G. V., Antokol'skaya, I. I. & Savvin, S. B. New chelating sorbents for noble metals.

        Talanta **32**, 1105–1112 (1985).

177.   Myasoedova, G. V., Savvin, S. B. & Blasius, E. Chelating sorbents in analytical chemistry. *C R C*

        Critical Reviews in Analytical Chemistry **17**, 1–63 (1986).

178.   Myasoedova, G. V. POLYORGS as complexing sorbents for preconcentration of trace metals.

        Fresenius J Anal Chem **341**, 586–591 (1991).

179.   Kantipuly, C., Katragadda, S., Chow, A. & Gesser, H. Chelating polymers and related supports for

        separation and preconcentration of trace metals. *Talanta* **37**, 491–517 (1990).

180.   Wu, T. *et al.* Amidoxime-functionalized macroporous carbon self-refreshed electrode materials

        for rapid and high-capacity removal of heavy metal from water. *ACS Cent. Sci.* **5**, 719–726 (2019).

181.   Morin, P.-O., Bura, T. & Leclerc, M. Realizing the full potential of conjugated polymers:

        innovation in polymer synthesis. *Mater. Horiz.* **3**, 11–20 (2016).

182.   Swager, T. M. *50th anniversary perspective* : conducting/semiconducting conjugated polymers.

        A personal perspective on the past and the future. *Macromolecules* **50**, 4867–4886 (2017).

183.   Whittell, G. R. & Manners, I. Metallopolymers: new multifunctional materials. *Adv. Mater.* **19**,

3439–3468 (2007).

184.   Su, X. & Hatton, T. A. Redox-electrodes for selective electrochemical separations. *Advances in*

Colloid and Interface Science **244**, 6–20 (2017).

185.   Su, X., Kulik, H. J., Jamison, T. F. & Hatton, T. A. Anion-Selective Redox Electrodes:

Electrochemically Mediated Separation with Heterogeneous Organometallic Interfaces. *Advanced*

Functional Materials **26**, 3394–3404 (2016).

186.   Kim, J., Kim, J. H. & Ariga, K. Redox-active polymers for energy storage nanoarchitectonics. *Joule*

1, 739–768 (2017).

187.   Su, X. & Hatton, T. A. Electrosorption at functional interfaces: from molecular-level interactions

to electrochemical cell design. *Phys. Chem. Chem. Phys.* **19**, 23570–23584 (2017).

188.   Vorotyntsev, M. A. & Vasilyeva, S. V. Metallocene-containing conjugated polymers. *Advances in*

Colloid and Interface Science **139**, 97–149 (2008).

189.   Burgess, M., Moore, J. S. & Rodríguez-López, J. Redox active polymers as soluble nanomaterials

for energy storage. *Acc. Chem. Res.* **49**, 2649–2657 (2016).

190.   Sengodu, P. & Deshmukh, A. D. Conducting polymers and their inorganic composites for

advanced Li-ion batteries: a review. *RSC Adv.* **5**, 42109–42130 (2015).

191.   Xing, J. *et al.* Electrically switched ion exchange based on polypyrrole and carbon nanotube

nanocomposite for the removal of chromium(VI) from aqueous solution. *Ind. Eng. Chem. Res.* **57**,

768–774 (2018).

192.   MacDiarmid, A. G. *et al.* The concept of `doping' of conducting polymers: the role of reduction

potentials [and discussion]. *Philosophical Transactions of the Royal Society A: Mathematical,*

Physical and Engineering Sciences **314**, 3–15 (1985).

193.   Ahonen, H. J., Lukkari, J. & Kankare, J. n- and p-doped poly(3,4-ethylenedioxythiophene): two

        electronically conducting states of the polymer. *Macromolecules* **33**, 6787–6793 (2000).

194.   Kiefer, D. *et al.* Double doping of conjugated polymers with monomer molecular dopants.

        Nature Mater **18**, 149–155 (2019).

195.   Liang, Z. *et al.* Influence of dopant size and electron affinity on the electrical conductivity and

        thermoelectric properties of a series of conjugated polymers. *J. Mater. Chem. A* **6**, 16495–16505

        (2018).

196.   Ibanez, J. G. *et al.* Conducting polymers in the fields of energy, environmental remediation, and

        chemical–chiral sensors. *Chem. Rev.* **118**, 4731–4816 (2018).

197.   Burgmayer, P. & Murray, R. W. Ion gate electrodes. Polypyrrole as a switchable ion conductor

        membrane. *J. Phys. Chem.* **88**, 2515–2521 (1984).

198.   Burgmayer, P. & Murray, R. W. An ion gate membrane: electrochemical control of ion

        permeability through a membrane with an embedded electrode. *J. Am. Chem. Soc.* **104**, 6139–6140

        (1982).

199.   Price, W. E., Too, C. O., Wallace, G. G. & Zhou, D. Development of membrane systems based on

        conducting polymers. *Synthetic Metals* **102**, 1338–1341 (1999).

200.   Zhao, H., Price, W. E. & Wallace, G. G. Synthesis, characterisation and transport properties of

        layered conducting electroactive polypyrrole membranes. *Journal of Membrane Science* **148**, 161–

        172 (1998).

201.   Davey, J. M., Ralph, S. F., Too, C. O., Wallace, G. G. & Partridge, A. C. Electrochemically

        controlled transport of metal ions across polypyrrole membranes using a flow-through cell. *Reactive

        and Functional Polymers* **49**, 87–98 (2001).

202.   Muhammad Ekramul Mahmud, H. N., Huq, A. K. O. & Yahya, R. binti. The removal of heavy metal

        ions from wastewater/aqueous solution using polypyrrole-based adsorbents: a review. *RSC Adv.* **6**,

        14778–14791 (2016).

203.   Rodríguez, F. J., Gutiérrez, S., Ibanez, J. G., Bravo, J. L. & Batina, N. The efficiency of toxic

        chromate reduction by a conducting polymer (polypyrrole): influence of electropolymerization

        conditions. *Environ. Sci. Technol.* **34**, 2018–2023 (2000).

204.   Lin, Y., Cui, X. & Bontha, J. Electrically controlled anion exchange based on polypyrrole and

        carbon nanotubes nanocomposite for perchlorate removal. *Environ. Sci. Technol.* **40**, 4004–4009

        (2006).

205.   Wen, L. & Kocherginsky, N. M. Doping-dependent ion selectivity of polyaniline membranes.

        Synthetic Metals **106**, 19–27 (1999).

206.   Mirmohseni, A., Price, W. E., Wallace, G. G. & Zhao, H. Adaptive membrane systems based on

        conductive electroactive polymers. *Journal of Intelligent Material Systems and Structures* **4**, 43–49

        (1993).

207.   Wang, J., Deng, B., Chen, H., Wang, X. & Zheng, J. Removal of aqueous Hg(II) by polyaniline:

        sorption characteristics and mechanisms. *Environ. Sci. Technol.* **43**, 5223–5228 (2009).

208.   Shao, D. *et al.* PANI/GO as a super adsorbent for the selective adsorption of uranium(VI).

        Chemical Engineering Journal **255**, 604–612 (2014).

209.   Higgins, S. J. Conjugated polymers incorporating pendant functional groups—synthesis and

        characterisation. *Chem. Soc. Rev.* **26**, 247–257 (1997).

210.   Agarwal, R. & Sharma, M. K. Selective electrochemical separation and recovery of uranium from

        mixture of uranium(VI) and lanthanide(III) ions in aqueous medium. *Inorg. Chem.* **57**, 10984–10992

        (2018).

211.   Shao, D. *et al.* PANI/GO as a super adsorbent for the selective adsorption of uranium(VI).

        Chemical Engineering Journal **255**, 604–612 (2014).

212.   Wang, Y., Astruc, D. & Abd-El-Aziz, A. S. Metallopolymers for advanced sustainable applications.

        Chem. Soc. Rev. **48**, 558–636 (2019).

213.   Eloi, J.-C., Chabanne, L., Whittell, G. R. & Manners, I. Metallopolymers with emerging

        applications. *Materials Today* **11**, 28–36 (2008).

214.   Gallei, M. & Rüttiger, C. Recent trends in metallopolymer design: redox-controlled surfaces,

        porous membranes, and switchable optical materials using ferrocene-containing polymers. (2018).

215.   Tian, W., Mao, X., Brown, P., Rutledge, G. C. & Hatton, T. A. Electrochemically nanostructured

        polyvinylferrocene/polypyrrole hybrids with synergy for energy storage. *Adv. Funct. Mater.* **25**,

        4803–4813 (2015).

216.   Espenscheid, M. W. & Martin, C. R. Ion exchange voltammetry with electroactive ionomers.

        Electroanalysis **1**, 93–95 (1989).

217.   Espenscheid, M. W. & Martin, C. R. Electroactive ion exchange polymers. *Journal of

        Electroanalytical Chemistry and Interfacial Electrochemistry* **188**, 73–84 (1985).

218.   Achilleos, D. S. & Hatton, T. A. Selective molecularly mediated pseudocapacitive separation of

        ionic species in solution. *ACS Appl. Mater. Interfaces* **8**, 32743–32753 (2016).

219.   Ren, Y., Mao, X. & Hatton, T. A. An asymmetric electrochemical system with complementary

        tunability in hydrophobicity for selective separations of organics. *ACS Cent. Sci.* **5**, 1396–1406

        (2019).

220.   He, F., Hemmatifar, A., Bazant, M. Z. & Hatton, T. A. Selective adsorption of organic anions in a

        flow cell with asymmetric redox active electrodes. *Water Research* 115963 (2020).

221.   Su, X. *et al.* Electrochemically-mediated selective capture of heavy metal chromium and arsenic

        oxyanions from water. *Nat Commun* **9**, 4701 (2018).

222.   Farmer, J. C. *et al.* Electrosorption of chromium ions on carbon aerogel electrodes as a means of remediating ground water. *Energy Fuels* **11**, 337–347 (1997).

223.   Nie, C. *et al.* Electrophoretic deposition of carbon nanotubes–polyacrylic acid composite film electrode for capacitive deionization. *Electrochimica Acta* **66**, 106–109 (2012).

224.   Jung, Y. *et al.* Enhanced electrochemical stability of a zwitterionic-polymer-functionalized electrode for capacitive deionization. *ACS Appl. Mater. Interfaces* **10**, 6207–6217 (2018).

225.   Gaikwad, M. S. & Balomajumder, C. Polymer coated capacitive deionization electrode for desalination: a mini review. *Electrochemical Energy Technology* **2**, (2016).

226.   Wang, Z. *et al.* Enhancement of heavy metals removal efficiency from liquid wastes by using potential-triggered proton self-exchange effects. *Electrochimica Acta* **130**, 40–45 (2014).

227.   Pascal, V., Laetitia, D., Joël, L., Marc, S. & Serge, P. New concept to remove heavy metals from liquid waste based on electrochemical pH-switchable immobilized ligands. *Applied Surface Science* **253**, 3263–3269 (2007).

228.   Viel, P. *et al.* Electropolymerized poly-4-vinylpyridine for removal of copper from wastewater. *Applied Surface Science* **212–213**, 792–796 (2003).

229.   Luo, T., Abdu, S. & Wessling, M. Selectivity of ion exchange membranes: A review. *Journal of Membrane Science* **555**, 429–454 (2018).

230.   Bakker, Eric., Meruva, R. K., Pretsch, Erno. & Meyerhoff, M. E. Selectivity of polymer membrane-based ion-selective electrodes: self-consistent model describing the potentiometric response in mixed ion solutions of different charge. *Anal. Chem.* **66**, 3021–3030 (1994).